

PerFACT: Motion Policy with LLM-Powered Dataset Synthesis and Fusion Action-Chunking Transformers

Davood Soleymanzadeh¹, Xiao Liang^{2,*}, and Minghui Zheng^{1,*}

Abstract—Deep learning methods have significantly enhanced motion planning for robotic manipulators by leveraging prior experiences within planning datasets. However, state-of-the-art neural motion planners are primarily trained on small datasets collected in manually generated workspaces, limiting their generalizability to out-of-distribution scenarios. Additionally, these planners often rely on monolithic network architectures that struggle to encode critical planning information. To address these challenges, we introduce Motion Policy with Dataset Synthesis powered by large language models (LLMs) and Fusion Action-Chunking Transformers (PerFACT), which incorporates two key components. Firstly, a novel LLM-powered workspace generation method, MotionGeneralizer, enables large-scale planning data collection by producing a diverse set of semantically feasible workspaces. Secondly, we introduce Fusion Motion Policy Networks (M π NetsFusion), a generalist neural motion planner that uses a fusion action-chunking transformer to better encode planning signals and attend to multiple feature modalities. Leveraging MotionGeneralizer, we collect 3.5M trajectories to train and evaluate M π NetsFusion against state-of-the-art planners, which shows that the proposed M π NetsFusion can plan several times faster on the evaluated tasks. Experimental evaluation videos are available via this [link](#).

Index Terms—Large Language Models (LLMs), Modality-aware Neural Motion Planning, Action Chunking Transformers (ACT), Fusion Transformers

I. INTRODUCTION

MOTION planning problem is a crucial component of the robotic manipulation stack, which involves finding a collision-free path between a start and goal configuration [1]. Traditional methods, like probabilistically complete sampling-based [2] and trajectory optimization [3] techniques, plan motions from scratch for each new problem. As a result, these methods consume a significant amount of time and computational resources and require privileged environmental knowledge.

Neural motion planners have been developed to enhance the performance of traditional motion planning algorithms [4]. These planners utilize various neural network architectures to encode the inherent structure within the planning problem to increase the efficiency of the motion planning algorithms. However, these planners are often trained on limited datasets collected in manually designed workspaces, which limits their ability to generalize to out-of-distribution planning scenarios.

This limitation is especially significant in motion planning for robotic manipulators, given the inherent discontinuities within the motion planning problems [5]. A small change in the workspace can induce significant changes in the configuration space that may not be present within the planning dataset [6]. As a result, large-scale datasets are required to establish general-purpose neural motion planners.

There are typically two approaches for synthesizing diverse workspaces to collect large-scale data and train general-purpose robotic systems. The first approach is procedural workspace generation [7], [8], which has specifically been used for training neural motion planners. This method employs basic shapes, and primitives to generate everyday objects of various sizes and configurations. Then, collision-aware random placement is leveraged to generate diverse workspaces for planning data collection. However, using random placement limits the diversity and semantic feasibility of the generated workspaces, which limits the generalizability of the neural motion planner to real-world environments.

The second approach leverages large language models (LLMs) for scene and task generation within manipulation autonomy stack [11]. Recognized for their advanced reasoning capabilities related to everyday human tasks [12], LLMs are increasingly used in robotic systems for high-level task planning [13]. These models are also being used to synthesize scenarios for robotic manipulation and locomotion [11]. In these scenarios, articulated objects are either sampled from existing 3D datasets [14], or are generated by state-of-the-art generative AI tools such as text-to-3D frameworks [15]. However, existing 3D datasets lack the diversity of everyday articulated objects in terms of shape and configuration, and generative AI tools also struggle to generate everyday objects with a high level of diversity, which limits the application of these methods for workspace generation for establishing generalist neural motion planners.

Additionally, state-of-the-art neural motion planners typically utilize current and goal robot configuration embeddings and workspace embeddings to predict the next planning state toward the goal, either for informed sampling [16] or end-to-end open-loop planning [8], [17]. These frameworks typically utilize simple feature concatenation to fuse and process configuration space (i.e., manipulator information) and workspace features (i.e., obstacle information), and perform feature-level fusion for motion planning [8], [16], [17]. This makes the learning process biased towards dominant planning modalities (e.g., workspace embeddings) and discards essential, yet sparse, planning signals (e.g., current and goal configuration embeddings).

In this work, we propose PerFACT, which contains two

¹Davood Soleymanzadeh and Minghui Zheng are with the J. Mike Walker '66 Department of Mechanical Engineering, Texas A&M University, College Station, TX 77843, USA (e-mail: davoodso@tamu.edu; mhzheng@tamu.edu).

²Xiao Liang is with the Zachry Department of Civil and Environmental Engineering, Texas A&M University, College Station, TX 77843 USA (e-mail: xliang@tamu.edu).

* Corresponding Authors.

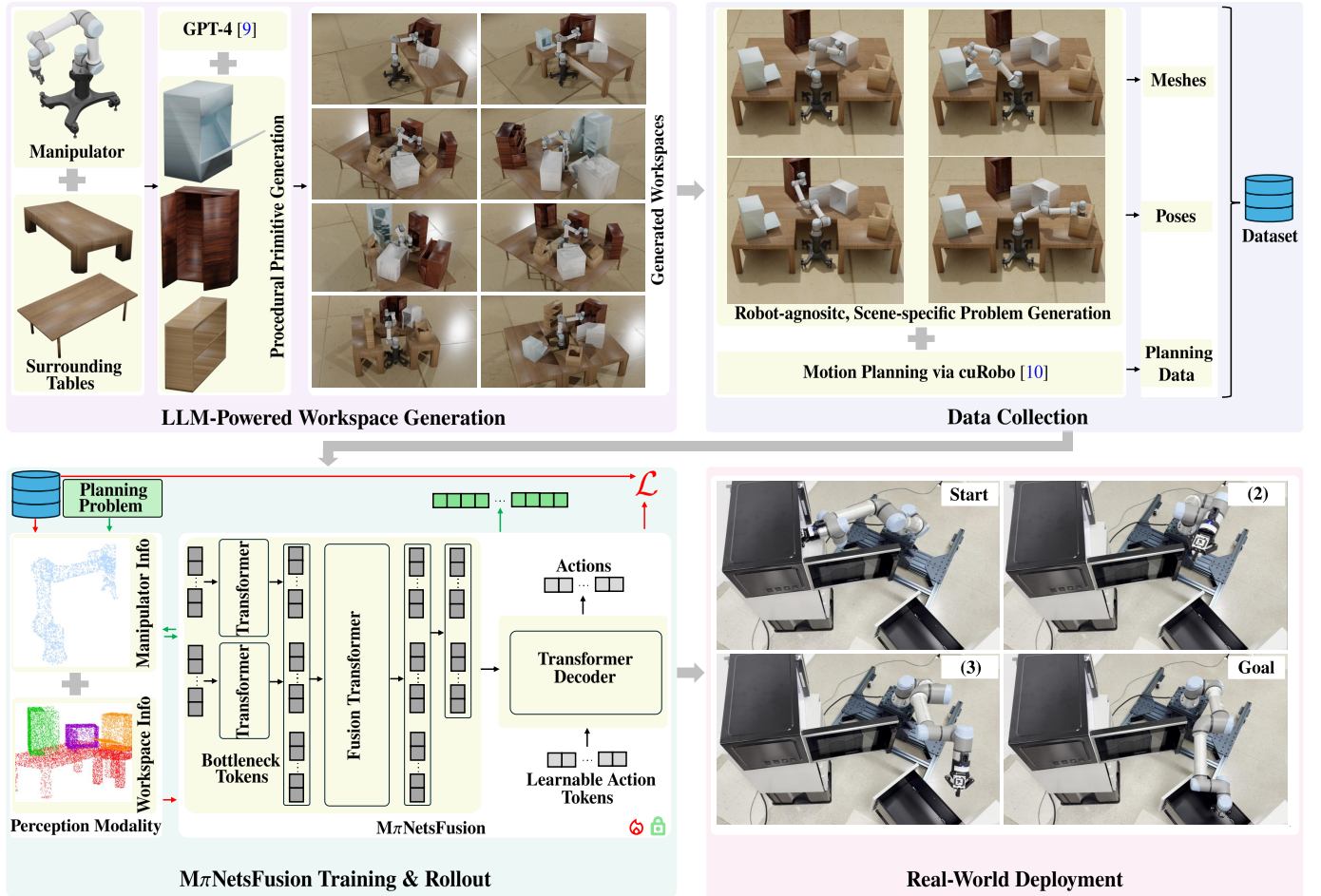


Fig. 1: PerFACT's various components and real-world deployment. Firstly, MotionGeneralizer (Section III) integrates procedural primitive generation with a large language model's (LLM) -GPT-4 [9]- reasoning capabilities to produce diverse workspaces for training generalist neural motion planners. Then, MotionGeneralizer generates robot-agnostic, scene-specific motion-planning problems (Section III-E) and integrates with state-of-the-art motion planners (cuRobo [10]) to generate a large-scale planning dataset. The dataset, combined with the perception modality (Section III-D) from MotionGeneralizer, is leveraged to train the $M\pi$ NetsFusion (Section IV). The sensing modality (Section III-D) is also utilized within the open-loop rollout of $M\pi$ NetsFusion to solve motion-planning problems in held-out evaluation scenarios (Section V). Finally, $M\pi$ NetsFusion is deployed within real-world planning scenarios (Section VI). The path profile from start configuration to the goal configuration is demonstrated in frames 2-3.

critical components to address the above-mentioned limitations of neural motion planners for robotic manipulators:

- A large-scale data collection framework called **MotionGeneralizer** (see Figure 1) which can provide diverse, semantically feasible workspaces for large-scale data collection and training general-purpose neural motion planners.
- A novel neural motion planner called **$M\pi$ NetsFusion** (See Figure 1) that utilizes motion planning modality-aware network architectures to attend to different planning feature modalities.

MotionGeneralizer is a novel framework that integrates procedural primitive generation with the reasoning capabilities of large language models (LLMs) to generate diverse planning workspaces. Procedural primitive generation is used to randomly generate various everyday articulated objects with different shapes and configurations, while an LLM is queried in a chain-of-thought (CoT) manner to get the number, position, and orientation of procedurally generated primitives for planning workspace generation. MotionGeneralizer provides

a method for large-scale dataset generation for establishing general-purpose neural motion planners for robotic manipulators.

The following are the main contribution of MotionGeneralizer:

- 1) MotionGeneralizer adopts procedural primitive generation frameworks from Neural MP [8], and NVIDIA SceneSynthesizer [18] to generate everyday objects commonly encountered by robotic manipulators in a household setting. Then, it prompts an LLM in a CoT manner to get the number of primitives per scene, and their corresponding position and orientation to generate semantically feasible workspaces. The strong, human-like reasoning capabilities of LLMs facilitate the creation of diverse, semantically feasible workspaces, which are crucial for compiling a large-scale, high-quality dataset to train general-purpose neural motion planners.
- 2) MotionGeneralizer generates a synthetic workspace point cloud by uniformly sampling points on obstacle meshes within the workspace, and on the robotic ma-

nipulator meshes at different configurations to improve spatial awareness and the success rate of neural motion planners. It also generates robot-agnostic, scene-specific motion planning problems by sampling collision-free poses within workspace primitives and the robotic manipulator’s reachable region. Any state-of-the-art motion planner, such as planners from Open Motion Planning Library (OMPL) [19] and cuRobo [10], can be used to collect planning data to solve these problems.

$M\pi$ NetsFusion is a novel planning framework that leverages a fusion transformer architecture to attend to different planning modalities and learn their inter-communications for effective motion planning. Specifically, it utilizes bottleneck transformers as the encoder within Action Chunking Transformers (ACT) [20] framework to learn and encode these cross-modal interactions. In this letter, planning modalities refer to feature information related to both the robotic manipulator and the workspace.

The following are the main contributions of $M\pi$ NetsFusion:

- 1) $M\pi$ NetsFusion employs bottleneck transformers [21], [22] to model the contribution of each planning modality to ensure that each modality contributes to the motion planning problem. The fusion encoder restricts information flow between planning modalities to ensure that only the most relevant and condensed representation from each planning modality is exchanged with other planning modalities.
- 2) Trained on a dataset generated by MotionGeneralizer, $M\pi$ NetsFusion is evaluated both in simulation, and real-world environments. The evaluation results demonstrate that it plans 4.47 times and 3.2 times faster than state-of-the-art sampling-based and neural motion planners, respectively.

The paper is organized as follows as demonstrated in Figure 1. Section II reviews related work on scene generation for planning data collection and neural motion planning for robotic manipulators. Section III presents MotionGeneralizer, describes its components, and compares it with state-of-the-art scene-generation methods. Section IV introduces the architecture of $M\pi$ NetsFusion motion planner. Section V evaluates and compares $M\pi$ NetsFusion with state-of-the-art sampling-based and neural motion planners, and provides ablation studies to analyze the contribution of its components to the successful planning. Section VI demonstrates real-world deployment of the proposed neural motion planner. Finally, Section VII concludes the paper.

II. RELATED WORK

In this section, we provide an overview of recent literature on the applications of LLMs in robotics and neural motion planners. We also highlight key distinctions between our research and the existing state of the art.

Data Scarcity in Neural Motion Planners: Neural motion planners utilize deep learning frameworks either for end-to-end motion planning [23] or to enhance the components of classical motion planning algorithms [4]. However, these models are trained on a small dataset generated from simple tabletop

or shelf workspaces, which leads to limited generalizability. A major challenge in using deep learning for low-level motion planning of robotic manipulators is data scarcity, which limits the generalization of these neural motion planners to out-of-distribution planning scenarios. MotionGeneralizer addresses the data scarcity of neural motion planners by providing a framework to generate cluttered and semantically feasible workspaces to collect a large-scale dataset.

Workspace/Environment Generation for Robotic Manipulation/Motion Planning: Roboticists have developed several frameworks to generate diverse and large-scale workspace/environments for learning motion and manipulation policies. One approach is using generative AI for 3D object/scene generation. Recent multi-modal generative AI approaches - such as *Text-to-3D Generation* [24] and *Image-to-3D Generation* [25] - can create realistic 3D assets and scenes [26]. Although these methods offer explicit and implicit object representations that could support automated workspace generation, generated objects lack the modular composability and articulation required for training generalist neural motion planners. MotionGeneralizer overcomes this limitation by programmatically generating articulated everyday objects.

Another approach is utilizing existing 3D Object Datasets for this purpose. Existing 3D object datasets - e.g., Objaverse [14] and PartNet-Mobility [27] - have been utilized in creating various environments for training generalist robotic manipulation policies in simulation [28]. However, these datasets lack articulated objects with diverse sizes and articulations required for motion planning. MotionGeneralizer fills this gap by programmatically generating everyday household primitives that vary in articulation and scale.

Another line of work utilizes procedural primitive generation for environment creation. These methods create everyday objects programmatically and place them randomly within the manipulator’s workspace for motion planning. MOTION-BENCHMARKER [7] generates workspaces either by randomly sampling from a nominal scene, or a URDF model. However, the resulting workspaces are not realistic and cluttered, as they only include one major obstacle, and other smaller obstacles are far apart. Motion Policy networks ($M\pi$ Nets) [17] generate their training data from only three workspace classes - tabletop scenes with randomly placed obstacles, cubbies, and dressers. Although this strategy yields a large dataset for the neural motion planner, the resulting scenes are simplistic and do not involve diverse configurations that robots may encounter in everyday applications.

Neural MP [8] addresses the limitations of MOTION-BENCHMARKER and $M\pi$ Nets by generating everyday objects with diverse sizes and shapes. It creates these objects by combining cuboid primitives and randomly placing them in the scene for workspace generation. While this procedural approach increases workspace diversity and facilitates data collection for general-purpose neural motion planners, it can sometimes create workspaces that are not semantically realistic due to the random placement procedure. MotionGeneralizer combines procedural primitive generation with high-level semantic planning of large language models (LLMs) to create

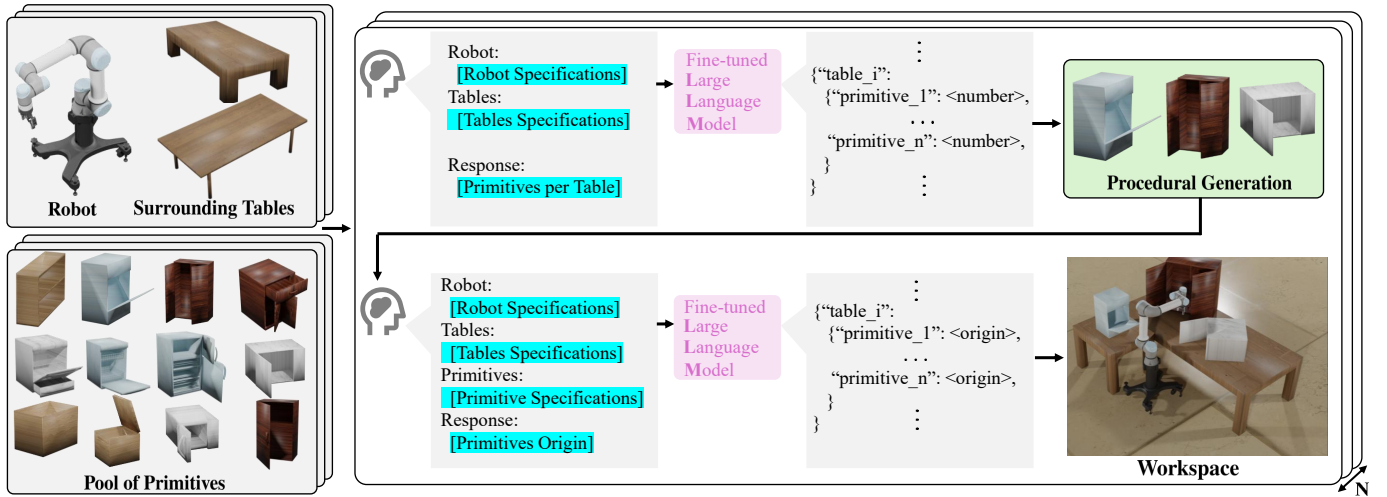


Fig. 2: MotionGeneralizer framework for diverse workspace generation. This method first randomly selects a robot type and the number of its surrounding tables, which are created using procedural generation. Next, it prompts the LLM in a few-shot manner (**Fine-tuned Large Language Model**) to determine the number of primitives for each table. The suggested primitives are then procedurally generated, given the pool of primitives, and the LLM is prompted again in a few-shot manner (**Fine-tuned Large Language Model**) to specify the location and orientation of each primitive on its respective table, and outputs the workspace. The procedure can be repeated to generate a diverse set of planning workspaces with an arbitrary number (N).

large-scale datasets for training generalist and scalable neural motion planners for robotic manipulators.

Language Models in Robotics: LLMs are trained on extensive internet-scale datasets and can be fine-tuned for various everyday tasks, such as in fluent text generation [9] and open-vocabulary visual recognition [29]. LLMs’ semantic reasoning, problem-solving, and visual interpretation capabilities have proven useful for establishing generalist robots [30], [31]. However, these models are mainly used for high-level robotic planning because these models mainly reason about semantics and textual prompts. LLMs’ application within low-level planning and control relies on additional auxiliary components, such as motion primitives [32] and motion optimizers [33], since these models are not inherently trained on physical interactions and trajectories [34].

Robotic Foundation Models: These models integrate LLMs and vision-language models (VLMs) into the low-level planning and control of robotic systems to achieve generalizability [35]. Also known as vision-language-action (VLA) models, these models are fine-tuned using a large robotics-related dataset [36] to facilitate zero-shot language-conditioned low-level control [35], [37]. However, a significant challenge remains in motion planning for robotic manipulators, as there is no large, robotics-specific dataset available for fine-tuning VLMs toward a general-purpose neural motion planning algorithm. MotionGeneralizer provides a framework to generate large-scale data with the potential of establishing manipulator planning foundation models.

Data-driven Motion Planning: Deep learning frameworks have been widely used to improve motion planning for robotic manipulators. These methods either enhance specific components of classical planners [4], [16] or function as end-to-end, open-loop planners [8], [17], [38]. They have been employed as informed samplers [4], [39]–[41] and collision

checkers [42]–[45] within sampling-based algorithms, used to learn constrained manifolds for constrained motion planning [46], [47], and applied to warm-start trajectory-optimization methods [48]–[51]. However, most existing approaches are trained on relatively small datasets derived from tabletop environments and therefore struggle to generalize to out-of-distribution scenarios. In contrast, MotionGeneralizer provides a workspace-generation workflow that enables the creation of large-scale, diverse datasets for training generalist neural motion planners.

Neural Motion Planners’ Architectures: The success of neural motion planners began with Motion Planning Networks (MPNets) and its variants [16], [52]–[54], where the robot’s current configuration, goal configuration, and workspace embeddings are concatenated as input features to a neural network that predicts the next time step configuration to construct a path towards the goal. Subsequent works, such as Motion Policy Networks (M π Nets), Neural MP [8], and Deep Reactive Policy [38] have extended this paradigm by leveraging a similar formulation to predict the next time step configuration within motion planning frameworks. These frameworks typically fuse multiple planning sensing modalities, such as current and goal configuration embeddings, current and goal robot point cloud embeddings, and workspace embeddings, via direct concatenation to predict the next time-step configurations towards the planning goal. However, since these global motion planners are mainly developed for static environments, the workspace point cloud often becomes the dominant and constant feature across diverse planning instances, which affects the performance of neural motion planners.

To address this limitation, Spatial-informed Motion Planning Networks (SIMPNet) [4] utilized a cross attention mechanism to attend to the workspace embedding, allowing the network to focus on other sparse yet critical planning modalities. Building upon SIMPNet, M π NetsFusion further enhances this

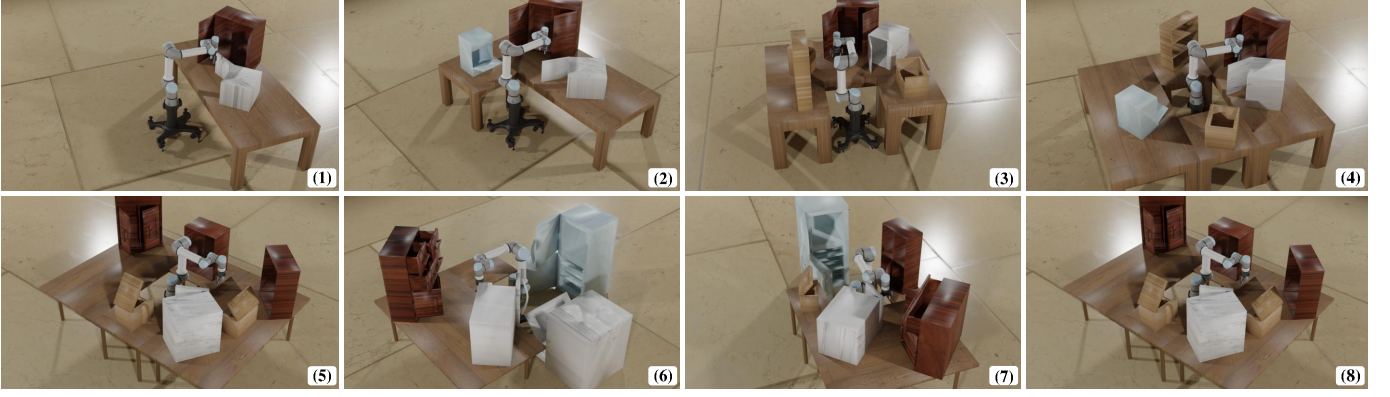


Fig. 3: Workspace generation: MotionGeneralizer can generate an arbitrary number of cluttered, semantically feasible workspaces given robotic manipulator type (UR5e) and a pool of everyday primitives.

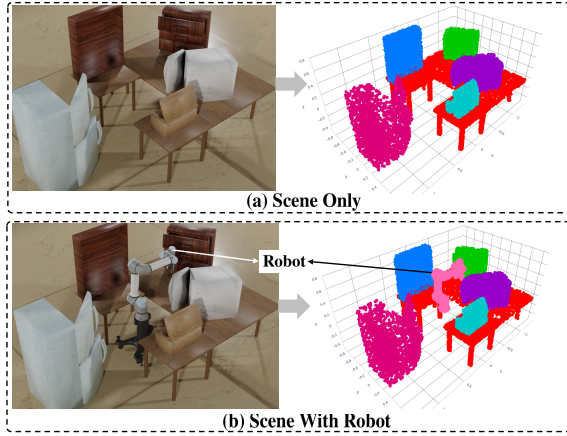


Fig. 4: Point Cloud Synthesis: MotionGeneralizer’s perception module provides a privileged point-cloud scene representation by uniformly sampling on workspace primitives (a) and robotic manipulator at arbitrary configurations (b) to increase spatial awareness for downstream planning tasks.

framework by employing a network architecture to adaptively attend to various planning sensing modalities for effective motion planning.

III. MOTIONGENERALIZER

In this section, we introduce MotionGeneralizer, which generates diverse and semantically feasible workspaces for training generalist neural motion planners. It first creates a variety of common articulated objects that a robotic manipulator may encounter in everyday tasks, and settings. Then, it leverages the reasoning capabilities of LLMs to generate feasible workspace configurations. MotionGeneralizer also includes sensing modality and manipulator-agnostic, scene-specific planning problem definition modules to enable data collection for robots with varying degrees of freedom. Figure 2 and Algorithm 2 illustrate the pipeline of the MotionGeneralizer framework.

A. Procedural Asset Generation

For procedural asset generation, MotionGeneralizer leverages methods from Neural MP [8], and NVIDIA’s SceneSynthesizer [18] framework.

Neural MP [8]: MotionGeneralizer utilizes the parameter ranges provided by Neural MP to procedurally generate everyday primitives, (e.g., tables, cabinets, dishwashers, microwaves, open boxes, and shelves). Using URDF sampling, it generates customized URDFs for each primitive based on the provided ranges, which enables the creation of articulated objects with diverse sizes and configurations. URDF sampling is a general framework with the potential of creating any articulated primitive given its parameter ranges.

NVIDIA’s SceneSynthesizer: MotionGeneralizer also incorporates procedurally generated articulated objects from SceneSynthesizer [18]. These objects originally include active revolute and prismatic joints designed for everyday manipulation tasks. To adapt them for motion planning, the active joints are fixed by assigning a random value within their original joint range. This approach generates a variety of primitives with diverse configurations.

B. Language-guided Workspace Generation

Manipulator and Table Selection: MotionGeneralizer first randomly selects a robotic manipulator from a pool of available manipulators with their reachability range, and randomly selects the number of tables to be placed around it. It then procedurally generates the required tables, using either Neural MP or the SceneSynthesizer framework, and places them within the manipulator’s reachability range.

Primitives per Table with LLM: SceneGeneralizer uses GPT-4 [9] to determine the number and types of objects (primitives) to place on each table towards semantically feasible workspace generation. The prompt sent to the language model includes details such as the robotic manipulator’s specifications, the number and surface areas of the tables, and a list of common household objects. Based on this information, the model outputs the quantity and types of primitives to place on each table. If fewer than four tables are generated, the LLM also suggests additional objects to place on the ground near the robot. This placement strategy ensures that the entire workspace is utilized, improving the diversity of planning scenarios and enhancing the generalizability of the neural motion planner.

Procedural Primitive Generation: Based on the types and

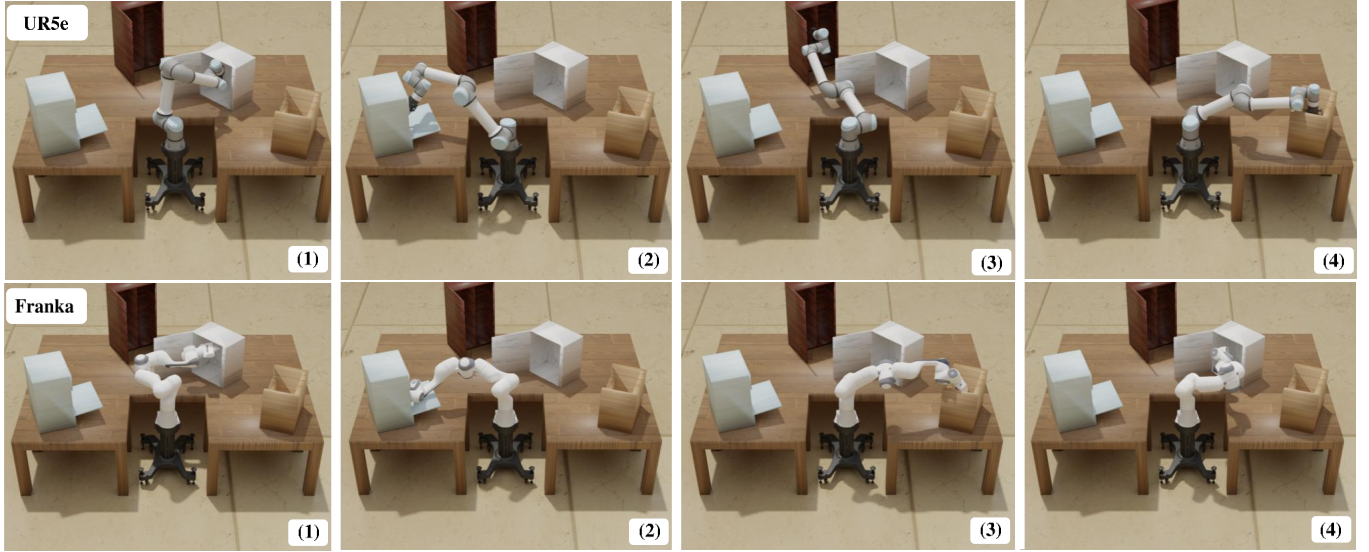


Fig. 5: Planning Problem Generation: MotionGeneralizer’s problem generator module provides robot-agnostic, scene-specific planning problem poses. Then, any arbitrary robotic manipulator, such as UR5e (top row) or Franka (bottom row), can use its collision-aware inverse kinematics to compute corresponding start-goal configurations of the planning problems.

quantities of primitives suggested by the LLM, SceneGeneralizer procedurally generates each object using either the NeuralMP or SceneSynthesizer primitive pools. This randomized generation process ensures that objects of the same type vary in size and configuration, promoting diversity in the workspace. Such variation improves the generalization capability of neural motion planners trained on these environments. In this stage, several instances of the same primitive can be procedurally generated to increase the number and variation of the generated workspaces.

Primitive Placement with LLM: Given the generated primitives on each table and on the ground, the LLM determines the position and orientation of each object relative to the local coordinate frame of the corresponding table. The prompt to the language model includes the robot specifications, table surface areas, and the dimensions of each primitive. Using this information, the LLM outputs semantically feasible placements by providing the position and orientation of each primitive in the local coordinate frame of the table.

Resolving Potential Collisions: SceneGeneralizer also performs a post-processing collision checking algorithm to detect and resolve any potential collisions in the workspace generated by the large language model. Figure 3 provides some examples of the generated workspaces with SceneGeneralizer.

C. Reducing Similarities Between Generated Workspaces

MotionGeneralizer already minimizes workspace similarity by randomly sampling the number of tables and generating individual primitives, introducing substantial variability (Section III-B). To further reduce overlap between workspaces, MotionGeneralizer introduces an additional framework that further reduces inter-workspace similarity, providing an extra layer of diversification for motion planning benchmarks.

This feedback framework leverages GPT-4 to generate a high-level, distinctive description of each workspace. The

prompt includes the number and type of primitives placed on each table and on the ground. Based on this input, the language model returns a concise textual description, which is then converted into an embedding vector. This embedding is compared against those of previously generated workspaces to measure similarity. If the similarity is below a predefined threshold, the workspace is accepted. Otherwise, MotionGeneralizer requests a new, more distinctive configuration from the language model.

D. Perception Modality

In real-world motion planning settings, the knowledge of precise geometries of obstacles are not known, and usually a sensed representation through RGB-D cameras may be available [55]. Also, the success of a neural motion planner is highly dependent on the encoding of inherent spatial correlations within the motion planning problem. Therefore, the most suitable sensing modality for capturing these spatial dependencies is high-dimensional point clouds. MotionGeneralizer provides a high-dimensional point cloud workspace observation for training neural motion planners and performing collision checking.

Utilizing multiple RGB-D cameras in simulation for point cloud rendering would consume a substantial amount of time, and the resulting point clouds would be occluded. Instead, MotionGeneralizer generates a synthetic workspace point cloud by uniformly sampling points on the surface of objects within the workspace (Figure 4 - (a)). This enables large-scale training of a privileged neural motion planner in simulation, which then can be fine-tuned with partial (occluded) camera-rendered point clouds before deployment in the real world [56].

M π Nets [17] and Neural MP [8] have demonstrated that sampling a point cloud on the robotic manipulator at each planning step, and including it as part of the perception modality, improves spatial awareness and the success rate of neural motion planners. To this end, MotionGeneralizer includes a framework for uniformly sampling points on the

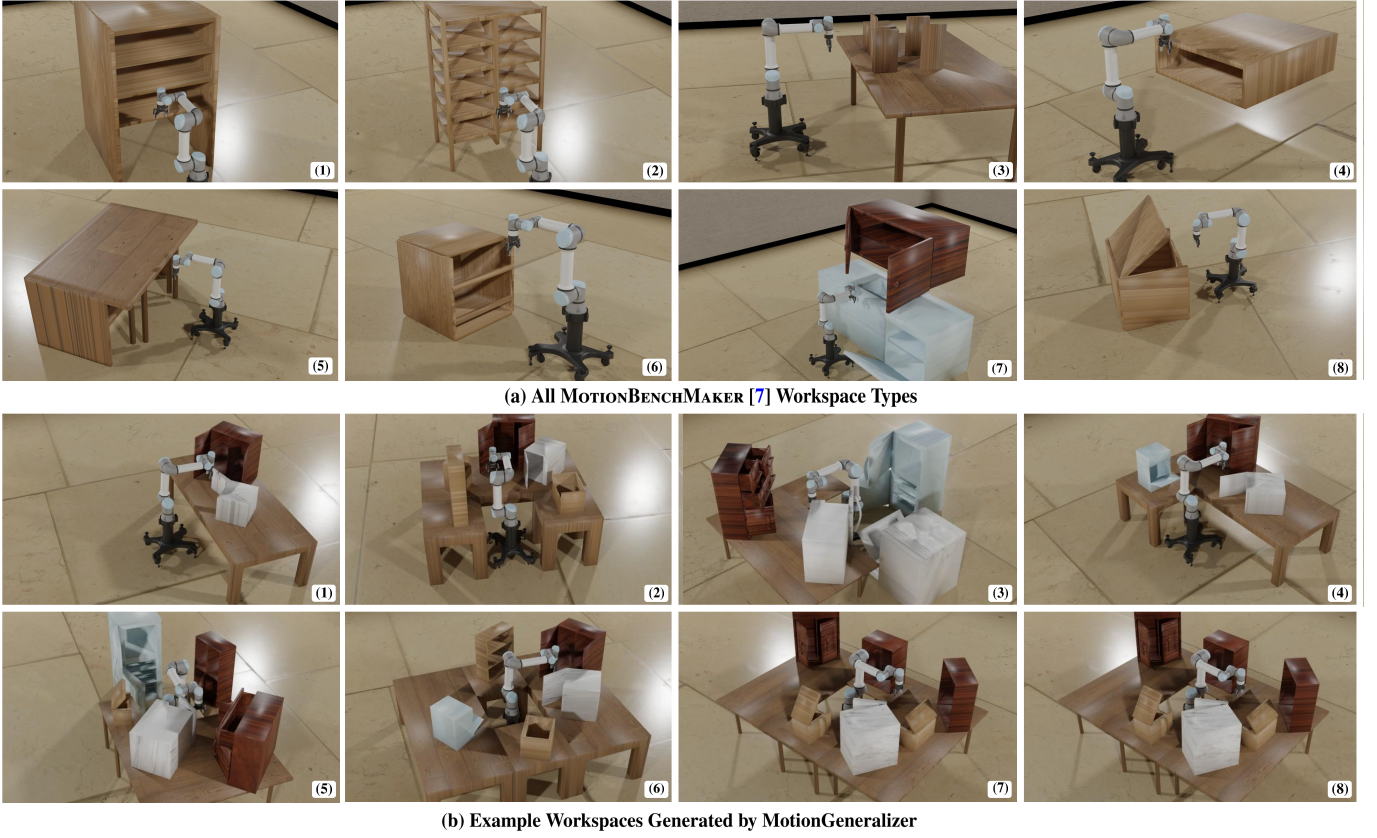


Fig. 6: MotionGeneralizer vs. MOTIONBENCHMAKER [7]: MOTIONBENCHMAKER only contains eight different workspaces with one major obstacle present (top). MotionGeneralizer can provide an arbitrary number of workspaces, and LLM determines the number of obstacles per scene (bottom - only 8 demonstrated for the sake of comparison), resulting in realistic and cluttered workspaces for robotic manipulator motion planning.

body of the robotic manipulators, as illustrated in Figure 4 - (b).

E. Motion Planning Problem Generator

In the literature, the main method for planning problem definition is to randomly generate start and goal pairs within the workspace. However, this often results in simple, not feasible cases where the robot can move in a straight line without maneuvering around obstacles [8]. Instead, MotionGeneralizer utilizes the shapes of generated primitives to provide scene-specific motion planning problems.

MotionGeneralizer generates robot-agnostic, scene-specific motion planning problems by sampling collision-free poses within the workspace, as demonstrated in Figure 5. Firstly, it samples collision-free poses within the workspace primitives and queries the collision-aware inverse kinematics of the given robotic manipulator to determine planning start and goal pairs within the configuration space. Additionally, it samples collision-free poses within a hemisphere constructed based on the given robotic manipulator’s reachability radius, and queries the collision-aware inverse kinematics to determine planning problems within the configuration space. Given the motion planning problem, any off-the-shelf motion planner (i.e., motion planners from OMPL [19], and cuRobo [10]) can be utilized to plan and collect dataset for training neural motion planners.

Algorithm 1: ProblemGenerator

```

1 Given: Generated workspaces: Workspaces.
2 Given: Collision checker: Q.
3 Given: Robot-specific collision-aware inverse kinematics: IK.
4 Given: Primitive pose sampler: PoseSampler.
5 Problems  $\leftarrow \emptyset$ 
6 for Workspace in Workspaces do
7   WorkspaceProblems  $\leftarrow \emptyset$ 
8   for Primitives in Workspace do
9     ProblemsPose  $\leftarrow \text{PoseSampler}(\text{Primitive}, \text{Pose})$ 
10    ProblemsConfig  $\leftarrow \text{IK}(\text{ProblemsPose})$ 
11    WorkspaceProblems  $\leftarrow \{\text{ProblemsConfig}\}$ 
12  Problems  $\leftarrow \{\text{WorkspaceProblems}\}$ 
13 return Problems

```

F. MotionGeneralizer vs. MOTIONBENCHMAKER

In this section, we qualitatively compare the workspaces generated by MOTIONBENCHMAKER [7] with ones created by MotionGeneralizer. MOTIONBENCHMAKER leverages SE(3) or URDF sampling to generate random workspaces.

SE(3) sampling perturbs the position and orientation of collision objects in a nominal scene to generate random

Algorithm 2: MotionGeneralizer

```

1 Given: Number of workspaces:  $N$ .
2 Given: Robotic manipulator: Manip.
3 Given: Number of tables:  $N_{\text{tab}}$ .
4 Given: Large language model: LLM [9].
5 Given: NeuralMP parameter ranges: NeuralMP [8].
6 Given: GenModes: NeuralMP or SceneSynth.
7 Given: SceneSynthesizer pool of primitives: [18].
8 Given: GenModes: NeuralMP or SceneSynth.
9 Given: Collision-free problem generator:
    ProblemGenerator (Algorithm 1).
10 Given: Primitive point cloud sampler: PCDSampler.
11 Given: Collision checker:  $Q$ .
12 Given: Collision Normal Calculator:  $Q_N$ .

13 Workspaces  $\leftarrow \emptyset$ 
14 PCDs  $\leftarrow \emptyset$ 
15 Problems  $\leftarrow \emptyset$ 
16 GenModel  $\leftarrow$  NeuralMP

    ▷ Generate workspaces
17 for  $i \leftarrow 0$  to  $N$  do
18   Workspace  $\leftarrow \emptyset$ 
    ▷ Generates tables
19   if GenMode is NeuralMP then
20     Tables  $\leftarrow$  NeuralMP( $N_{\text{tab}}$ )
21   else
22     Tables  $\leftarrow$  SceneSynth( $N_{\text{tab}}$ )
    ▷ Query LLM to get #primitives per table
23   #TablePrimitives  $\leftarrow$  LLM(Manip, Tables)
    ▷ Procedurally generate primitives
24   if GenMode is NeuralMP then
25     Primitives  $\leftarrow$  NeuralMP(#TablePrimitives)
26   else
27     Primitives  $\leftarrow$  SceneSynth(#TablePrimitives)
    ▷ Query LLM to get each primitive pose
28   PrimitivesPose  $\leftarrow$  LLM(Tables, Primitives, Manip)
    ▷ Collision checking
29   for Primitive in Primitives do
30     while  $Q(\textit{Workspace}, \textit{Primitive})$  do
31       for Primitivei in Workspace do
32          $n_i \leftarrow Q_N(\textit{Workspace}, \textit{Primitive})$ 
33          $n \leftarrow \sum n_i$ 
34         PrimitivePose  $\leftarrow$  PrimitivePose +  $n$ 
35       Workspace  $\leftarrow \{\textit{Primitive}\}$ 
36   Workspaces  $\leftarrow \{\textit{Workspace}\}$ 

    ▷ Perception modality
37 for Workspace in Workspaces do
38   WorkspacePCD  $\leftarrow \emptyset$ 
39   for Primitive in Workspace do
40     PrimitivePCD  $\leftarrow$  PCDSampler(Primitive, Pose)
41     WorkspacePCD  $\leftarrow \{\textit{PrimitivePCD}\}$ 
42   PCDs  $\leftarrow \{\textit{WorkspacePCD}\}$ 

    ▷ Planning problem generation
42 Problems  $\leftarrow$  ProblemGenerator(Workspaces)

```

workspaces. The nominal values act as the mean of the sampling distribution, while the variance or uniform bounds are selected from a predefined range. In contrast, URDF sampling generates variability by sampling configurations from the nominal scene's URDF. Since the URDF includes articulated objects with movable joints (e.g., cabinet or dishwasher doors), selecting random values within the joint limits produces workspaces with different articulations.

As demonstrated in Figure 6, MotionBenchmark generates simple workspaces containing only a single major obstacle. As a result, the generated workspaces are not realistic, and neural motion planners trained on these struggle to plan within real-world environments.

IV. M π NETSFUSION

In this section, we introduce M π NetsFusion, an end-to-end neural motion planner that utilizes the robot's current and goal configurations, the manipulator's point cloud, and the workspace point cloud to generate a feasible trajectory connecting given start and goal configurations.

A. Motion Planning Definition

Let $\mathcal{C} \in \mathbb{R}^n$ denote the configuration space of a robotic manipulator, representing an n -dimensional space spanned by its joint values. This space consists of two regions: the obstacle space ($\mathcal{C}_{\text{obs}} \subset \mathcal{C}$), and the free space ($\mathcal{C}_{\text{free}} = \mathcal{C} \setminus \mathcal{C}_{\text{obs}}$). The objective of motion planning is to find a feasible path that connects the start and goal configurations while remaining entirely within the free space. Given a start configuration ($\mathbf{q}_{\text{start}} \in \mathcal{C}_{\text{free}}$), and a goal configuration ($\mathbf{q}_{\text{goal}} \in \mathcal{C}_{\text{free}}$), the goal is to find a feasible path $\sigma = [\mathbf{q}_1, \dots, \mathbf{q}_t, \dots, \mathbf{q}_T]$ such that:

$$\begin{aligned}
 \sigma(0) &= \mathbf{q}_{\text{init}}, \\
 \sigma(t) &\in \mathcal{C}_{\text{free}}, \\
 \sigma(T) &= \mathbf{q}_{\text{goal}}.
 \end{aligned} \tag{1}$$

B. Planning via Action Chunking

Previous research has demonstrated [20], [57] that predicting action chunks [58] (A) effectively preserves temporal action consistency and handles non-Markovian actions. Inspired by the success of concurrent work [38], we also utilize an action chunking encoder-decoder framework for motion planning. Figure 7 demonstrates the structure of M π NetsFusion motion planner.

C. M π NetsFusion Components

Embedding Current and Goal Configurations: At first, a shared multi-layer perceptron (MLP) is utilized to tokenize the current and goal configurations as follows:

$$\mathbf{z}_t = \text{MLP}_I(\mathbf{q}_t), \tag{2}$$

$$\mathbf{z}_{\text{goal}} = \text{MLP}_I(\mathbf{q}_{\text{goal}}), \tag{3}$$

where $\mathbf{q}_t \in \mathbb{R}^6$, $\mathbf{q}_{\text{goal}} \in \mathbb{R}^6$, $\mathbf{z}_t \in \mathbb{R}^H$, and $\mathbf{z}_{\text{goal}} \in \mathbb{R}^H$ are current time-step configuration, goal configuration, current time-step configuration embedding, and goal configuration embedding, respectively.

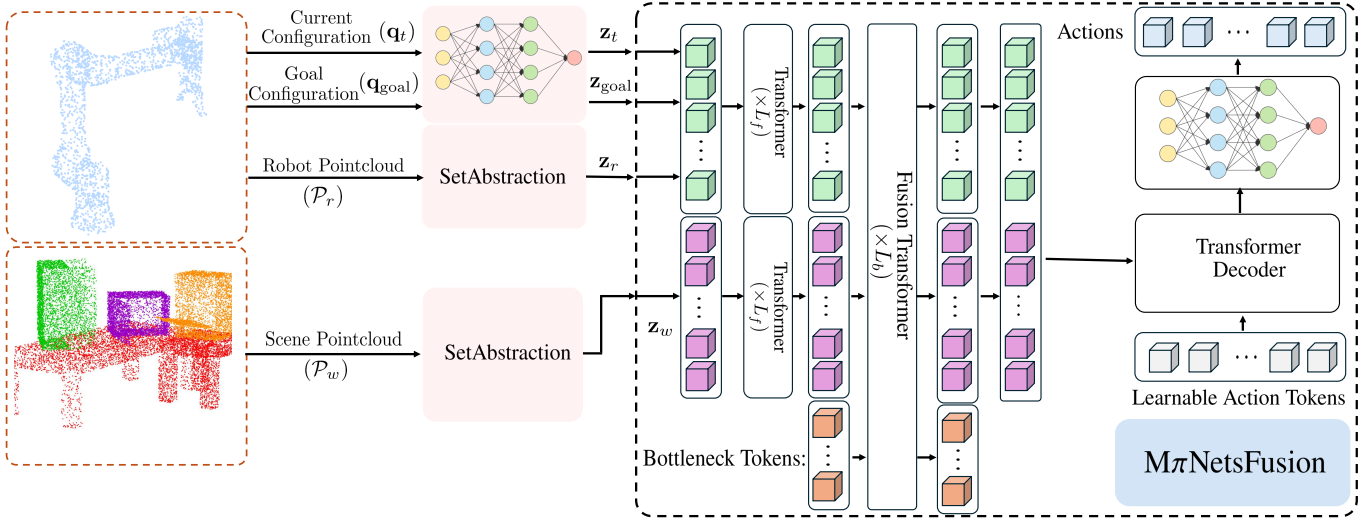


Fig. 7: M π NetsFusion Network Architecture: The framework leverages current-time-step workspace information (including the workspace and robot point clouds) together with configuration space features (current-time-step and goal configuration) to generate an action sequence that guides the robotic manipulator toward the motion planning goal. \mathbf{z}_t , \mathbf{z}_{goal} , \mathbf{z}_r , and \mathbf{z}_w are the current time-step configuration, planning goal configuration, robot point cloud, and scene point cloud embeddings, respectively. L_f is the number of unimodal transformer layers, and L_b is the number of fusion transformer layers.

Embedding Robot and Workspace Point Clouds: The robotic manipulator and scene point clouds can be generated either by uniformly sampling points on the object meshes in simulation or using RGB-D cameras during real-world deployment. We utilize set abstraction layers from PointNet++ [59] to down-sample and tokenize these point clouds as follows:

$$\mathbf{z}_r = \text{SetAbstraction}(\mathcal{P}_r), \quad (4)$$

$$\mathbf{z}_w = \text{SetAbstraction}(\mathcal{P}_w), \quad (5)$$

where $\mathcal{P}_r \in \mathbb{R}^{N_r \times 3}$, $\mathcal{P}_w \in \mathbb{R}^{N_w \times 3}$, $\mathbf{z}_r \in \mathbb{R}^{K_r \times H}$, and $\mathbf{z}_w \in \mathbb{R}^{K_w \times H}$ are robot point cloud, scene point cloud, robot point cloud embedding, and scene point cloud embedding, respectively.

Transformer Encoder: After encoding all planning modalities, we concatenate all robot-related modalities as follows:

$$\mathbf{z}_{\text{robot}} = [\mathbf{z}_t \parallel \mathbf{z}_{\text{goal}} \parallel \mathbf{z}_r], \quad (6)$$

where $\mathbf{z}_{\text{robot}} \in \mathbb{R}^{(K_r+2) \times H}$ is robot embedding. Afterwards, we utilize positional encoding to retain the positional information of transformer encoder inputs, given that transformers are agnostic to the spatial locations of their inputs [60]. The common solution is to add learned or fixed vectors to encode the position of each input [22]. We utilize a fixed vector as positional encoding as follows:

$$\text{PE}(\text{pos}, 2i) = \sin\left(\frac{\text{pos}}{10000^{\frac{2i}{H}}}\right), \quad (7)$$

$$\text{PE}(\text{pos}, 2i+1) = \cos\left(\frac{\text{pos}}{10000^{\frac{2i}{H}}}\right), \quad (8)$$

where pos and i are the position and dimension, respectively. After applying positional encoding, each planning modality can be represented as follows:

$$\mathbf{z}_{\text{robot}} = [\mathbf{z}_{\text{robot}} + \mathbf{p}_{\text{robot}}], \quad (9)$$

$$\mathbf{z}_w = [\mathbf{z}_w + \mathbf{p}_w], \quad (10)$$

where $\mathbf{p}_{\text{robot}} \in \mathbb{R}^{(K_r+2) \times H}$, and $\mathbf{p}_w \in \mathbb{R}^{K_w \times H}$ are positional encodings for each planning sensing modalities.

Instead of performing pair-wise attention between planning sensing modalities, we introduce a set of fusion bottleneck tokens to the transformer encoder input sequence as follows:

$$\mathbf{z} = [\mathbf{z}_{\text{robot}} \parallel \mathbf{z}_w \parallel \mathbf{z}_{\text{fusion}}], \quad (11)$$

where $\mathbf{z}_{\text{fusion}} = [\mathbf{z}_{\text{fusion}}^1, \dots, \mathbf{z}_{\text{fusion}}^B] \in \mathbb{R}^{B \times H}$ is fusion bottleneck tokens. Then, the cross-attention between different planning sensing modalities in each transformer layer (l) is performed via these fusion bottleneck tokens as follows:

$$[\mathbf{z}_i^{l+1} \parallel \hat{\mathbf{z}}_{\text{fusion}_i}^{l+1}] = \text{TransformerEncoder}([\mathbf{z}_i^l \parallel \hat{\mathbf{z}}_{\text{fusion}_i}^l]; \theta_i), \quad (12)$$

$$\mathbf{z}_{\text{fusion}}^{l+1} = \frac{\sum_{i=1}^B \hat{\mathbf{z}}_{\text{fusion}_i}^{l+1}}{B}, \quad (13)$$

where i and θ_i are planning modality indexes, and network parameters, respectively. These bottleneck tokens distill and transform information between different planning sensing modalities within each transformer encoder layer. Then, we utilize a concatenation operator to aggregate the processed information from each modality, serving as the memory for the transformer decoder.

Transformer Decoder: The transformer decoder follows a standard transformer architecture, conditioned on the output of the transformer encoder to predict a motion planning action sequence. It takes as input a set of learnable action tokens ($S \in \mathbb{R}^{A \times H}$) and uses the encoder output as memory to generate a sequence of delta joint actions $[\delta \bar{\mathbf{q}}_1, \delta \bar{\mathbf{q}}_2, \dots, \delta \bar{\mathbf{q}}_A] \in \mathbb{R}^{A \times 6}$, which are then converted into joint targets and executed by the robotic manipulator's low-level controller.

Table I presents the architecture of M π NetsFusion. The design follows the concurrent architecture proposed in [38], considering its demonstrated effectiveness for motion planning.



Fig. 8: Simulation evaluation: π NetsFusion planning in held-out planning task and an out-of-distribution **Scene** (bottom row) generated by MotionGeneralizer with planning time of 0.2 \sim 0.3 seconds. The path profile from start configuration to the goal configuration is demonstrated through frames 2-4.

TABLE I: $M\pi$ NetsFusion architecture & hyperparameters. “PCD” stands for point cloud, and “MHSA” stands for multi-head self-attention.

Hyperparameter	Value	Hyperparameter	Value
TransformerFusion Parameters		Input Parameters	
Scene-PCD Tokens (K_w)	2048	Scene-PCD (P_w)	2048
Robot-PCD Tokens (K_r)	256	Robot-PCD (P_r)	256
Unmodal Layers (L_f)	3	SetAbstraction Layer	
Bottleneck Layers (L_b)	3	Radius	0.1
Bottleneck Tokens (B)	4	Samples	64
Decoder Layers	6	MLP Hidden Layers	[64, 64, 64]
MHSA Heads	8	Current/Target Joint Configuration Encoder	
Hidden Dim	128	MLP Hidden Layers	[128, 256]
Feed-Forward Dim	1024		
Action Chunk	10		

V. RESULTS AND DISCUSSIONS

In this section, we detail the implementation of $M\pi$ NetsFusion and compare its performance with state-of-the-art sampling-based, and neural motion planners. All the frameworks are developed using the PyTorch framework [61], and the simulation evaluations were conducted on a

computer running Linux OS, equipped with NVIDIA RTX 4080 GPU.

A. Data Collection

We leveraged MotionGeneralizer (Section III) to create a diverse set of semantically feasible workspaces, and motion planning problems, and then we leverage cuRobo [10], a GPU-accelerated optimization-based motion planner, to solve the planning problems and collect a large-scale dataset of 3.5M trajectories for training the proposed neural motion planner.

B. $M\pi$ NetsFusion Training

We utilize $M\pi$ NetsFusion parameterized by θ for end-to-end planning. Let $[\delta \mathbf{q}_1, \delta \mathbf{q}_2, \dots, \delta \mathbf{q}_A] \in \mathbb{R}^{A \times 6}$ be the ground-truth delta joint actions from the planning dataset \mathcal{D} , the training loss function is defined as:

$$\mathcal{L}_{M\pi\text{NetsFusion}} = \frac{1}{A} \sum_{i=1}^A \|\delta \mathbf{q}_i - \delta \bar{\mathbf{q}}_i\|^2 \quad (14)$$

where $\delta \bar{\mathbf{q}}_i$ is the delta joint action predicted by the network. We train a 4.15M parameter model on a dataset of 3.5M

trajectories. The network is optimized using an MSE loss for 1.6M gradient steps, which requires wall-clock time of one day of training on a single NVIDIA A100 GPU with a batch size of 256.

C. $M\pi$ NetsFusion Planning

$M\pi$ NetsFusion is evaluated in an open-loop manner, similar to the state-of-the-art end-to-end neural motion planners [17], [62]. The planning policy is rolled out for a fixed number of steps, where each predicted joint action chunks is recursively fed back as input for subsequent action joint predictions. Planning success is defined as the end-effector reaching within a predefined threshold of the planning problem’s goal-pose configuration while avoiding collisions with the environment. Algorithm 3 summarizes motion planning with $M\pi$ NetsFusion.

D. Baselines

We assess the performance of $M\pi$ NetsFusion by comparing it with state-of-the-art motion planners. The baseline motion planners are as follows:

- **Adaptively Informed Trees (AIT*)** [63]: AIT* is an asymptotically optimal sampling-based motion planning algorithm that utilizes informed heuristic sampling to build a planning tree towards the goal.
- **Motion Planning Networks (MPNets)** [16]: MPNets is a neural informed sampler that generates informed (goal-directed, collision-free) samples within the framework of sampling-based motion planners. We implemented MPNets based on the official implementation code, and modify it to be compatible with our UR5e robotic manipulator.
- **Spatial-informed Motion Planning Network (SIMP-Net)** [4]: SIMPNet is a kinematics-aware neural sampler that generates informed samples towards the planning goal. This framework utilizes a cross-attention mechanism to condition the sampling network on workspace embeddings for collision-aware, goal-directed sample generation.
- **Neural MP** [8]: Neural MP is an end-to-end neural motion planner that plans in an open-loop manner. This framework utilizes a Recurrent Neural Network (RNN)-based decoder to learn the temporal dependencies within the motion planning problems, as well as a Gaussian Mixture Model (GMM) head to encode the probabilistic and multi-modal nature of sampling-based motion planning algorithms. We adopt Neural MP’s base policy based on the official implementation code and adapt it to be compatible with our UR5e robotic manipulator.

E. Evaluation Metrics

We use three planning metrics throughout the paper to evaluate the performance of $M\pi$ NetsFusion against benchmark planners and in ablation studies: *planning time*, *goal reaching*, and *success rate*. *Planning time* “ T ” denotes the average planning time the planner takes in each workspace. *Goal reaching* “ N_r ” refers to the percentage of planned paths reached the goal in each environment, regardless of collision status. *Success rate*

Algorithm 3: $M\pi$ NetsFusion Planning

```

1 Given: Trained  $M\pi$ NetsFusion:  $\pi_\theta$ .
2 Given: Roll-out length  $T$ .
3 Given: Planning success thresholds:  $\Delta_{pos}$ ;  $\Delta_{quat}$ .
4 Given: Forward kinematics function:  $FK$ .
5 Given: Collision checker:  $Q$ .
6 Given: Start and goal configurations:  $\mathbf{q}_{start}$ ;  $\mathbf{q}_{goal}$ .
7 Given: Scene point cloud, and robot point cloud
  sampler: ScenePCD, PCDSampler.
8  $pos_g, quat_g \leftarrow FK(\mathbf{q}_{goal})$ 
9  $Trajectory \leftarrow \emptyset$ 
10  $RolledPolicy \leftarrow \{\mathbf{q}_{start}\}$ 
11  $ReachedGoal \leftarrow False$ 
12  $Success \leftarrow False$ 
13  $\mathbf{q}_t \leftarrow \mathbf{q}_{start}$ 
  ▷ Rolling policy
14 for  $i \leftarrow 0$  to  $T$  do
  |   ▷ Sample point cloud
  |    $RobotPCD \leftarrow PCDSampler(\mathbf{q}_t)$ 
  |    $\delta\mathbf{q}_{t:t+a} \leftarrow \pi_\theta(\mathbf{q}_t, \mathbf{q}_{goal}, RobotPCD, ScenePCD)$ 
  |   for  $\delta\mathbf{q}$  in  $\delta\mathbf{q}_{t:t+a}$  do
  |   |    $\mathbf{q}_t \leftarrow \mathbf{q}_t + \delta\mathbf{q}$ 
  |   |    $RolledPolicy \leftarrow Add(\mathbf{q}_t)$ 
  ▷ Reaching goal
20 for  $\mathbf{q}$  in  $RolledPolicy$  do
21 |    $Trajectory \leftarrow Add(\mathbf{q})$ 
  |   ▷ forward kinematics
22 |    $pos, quat \leftarrow FK(\mathbf{q})$ 
23 |    $\delta_{pos} \leftarrow Distance(pos, pos_g)$ 
24 |    $\delta_{quat} \leftarrow Distance(quat, quat_g)$ 
25 |   if  $\delta_{pos} \leq \Delta_{pos}$  and  $\delta_{quat} \leq \Delta_{quat}$  then
26 |   |   return  $Trajectory$ 
27 |   else
28 |   |   return  $\emptyset$ 
  ▷ Collision checking
29 if  $Trajectory$  then
30 |    $CollisionFree \leftarrow Q(Trajectory)$ 
31 |   if  $CollisionFree$  then
32 |   |   return  $Trajectory$ 
33 |   else
34 |   |   return  $\emptyset$ 
35 return  $\emptyset$ 

```

“ S ” represents the percentage of successfully planned paths in each workspace.

F. Evaluation Tasks

We created several held-out planning environments in simulation for evaluating the performance of $M\pi$ NetsFusion compared to the benchmark planners. These evaluation tasks are as follows:

- **TableTop:** This task is adapted from MOTIONBENCH-MAKER [7] and consists of a tabletop environment with

TABLE II: Planning performance of $M\pi$ NetsFusion and baseline planners across all held-out planning task environments. “T” denotes *planning time*, and “S” refers to *success rate*. \downarrow indicates lower is better, and \uparrow indicates higher is better.

	TableTop		Box		Bins		Shelf					
							Task I		Task II		Task III	
	T [s] \downarrow	S [%] \uparrow	T [s] \downarrow	S [%] \uparrow	T [s] \downarrow	S [%] \uparrow	T [s] \downarrow	S [%] \uparrow	T [s] \downarrow	S [%] \uparrow	T [s] \downarrow	S [%] \uparrow
AIT* [63]	1.02 \pm 0.0	31%	1.02 \pm 0.0	57%	1.02 \pm 0.0	69%	1.02 \pm 0.0	42%	1.02 \pm 0.0	27%	1.2 \pm 0.0	27%
MPNets [16]	5.79 \pm 9.2	49%	2.8 \pm 1.69	67.3%	3.63 \pm 1.25	84.2%	3.39 \pm 5.44	40%	2.68 \pm 1.06	34%	7 \pm 4.7	32%
SIMPNet [4]	4.54 \pm 5.32	67%	2.2 \pm 2.34	88.6%	3.55 \pm 1.71	95%	2.21 \pm 1.25	44%	2.57 \pm 0.89	35%	3.44 \pm 1.19	33%
NeuralMP [8]	0.7 \pm 0.0	4%	0.72 \pm 0.03	19%	0.74 \pm 0.06	27%	0.72 \pm 0.04	14%	0.7 \pm 0.01	11%	0.73 \pm 0.0	13%
$M\pi$NetsFusion	0.22\pm0.01	58%	0.23\pm0.05	61.3%	0.24\pm0.04	84.5%	0.24\pm0.03	35.7%	0.22\pm0.01	34.6%	0.22\pm0.01	33.4%

TABLE III: Average success rate and time comparison of $M\pi$ NetsFusion with benchmark planners across all held-out planning tasks. “Fusion” denotes $M\pi$ NetsFusion.

	AIT*	MPNets	SIMPNet	NeuralMP	$M\pi$NetsFusion
S [%]	42.1%	51%	51.8%	14.6%	51.2%
$\frac{T}{T_{\text{Fusion}}}$	TableTop	4.63	26.31	20.5	3.5
	Box	4.43	12.17	9.56	3.13
	Bins	4.25	15.12	14.79	3.08
	Shelf I	4.25	14.12	9.20	3.0
	Shelf II	4.63	12.18	11.68	3.18
	Shelf III	4.63	31.81	15.63	3.31
	Average	4.47	18.61	13.56	3.2

various obstacles placed on it in front of the robot. The goal is to plan collision-free motions around and in-between these obstacles.

- **Box:** This task is also adapted from MOTIONBENCHMAKER [7], which consists of a box placed in front of the robotic manipulator at arbitrary positions and orientations. The planning problems require the robot to generate collision-free motions to reach inside the box, to evaluate its ability to transition between free space and tight, confined regions.
- **Bins:** This task is adapted from Neural MP framework [8] and consists of two bins placed in front of the robot at arbitrary positions and orientations. The planning problems require the robot to move between the bins to evaluate motion planners’ ability to transition between two tight spaces.
- **Shelf I, II & III:** These tasks are adapted from MOTIONBENCHMAKER [7] and Neural MP [8], and consist of shelves placed in front of the robot at arbitrary configurations. They evaluate the ability of motion planners to maneuver between and around shelf rungs.

G. Evaluation Results

Table II shows the performance of the considered planners across these held-out planning environments, while Table III provides the average success rate and time comparison of the proposed planner with benchmark planners across all held-out planning tasks. Also, Figure 8 provides an example of policy roll-out for all the evaluation tasks in simulation.

$M\pi$ NetsFusion achieves comparable performance to AIT* (51.2% vs. 42.1%) while plan 4.47 times faster on average.

This improvement can be attributed to the fact that AIT* requires a collision checker to plan and iteratively check the collision of sampled states, whereas $M\pi$ NetsFusion plans end-to-end, using only the planning start configuration, goal configuration, and the workspace point cloud.

$M\pi$ NetsFusion also performs comparably to benchmark neural samplers. Its achieves a success rate of 51.2% versus 51% for MPNets and 51.8% for SIMPNet, while planing 18.61 and 13.56 times faster, respectively. MPNets flattens and concatenates configuration-space and workspace point cloud embeddings to predict the next configuration state towards the planning goal. Its learned sampling primitive is embedded within a closed-loop, bidirectional planner that falls back to replanning when two consecutive states cannot be connected. Consequently, MPNets relies on a collision-checker for both planning and replanning, resulting in larger planning times. SIMPNet leverages the kinematic structure of the robotic manipulator and employs a cross-attention mechanism to combine planning modalities from workspace and configuration space to predict the next time step configuration state towards the goal. However, similar to MPNets, SIMPNet is also embedded within a bi-directional, closed-loop planner that requires a collision checker, resulting in longer planning times.

$M\pi$ NetsFusion also outperforms NeuralMP’s base planning policy (51.2% versus 14.6%) while planning 3.2 times faster on average across all planning tasks. Although NeuralMP’s base policy is also an open-loop, end-to-end planner that does not rely on a collision checker, it concatenates configuration-space and workspace planning modalities. This causes the workspace point cloud to dominate the feature representation, resulting in a lower overall success rate. Moreover, NeuralMP’s base policy predicts only the next delta joint angles, whereas $M\pi$ NetsFusion predicts an action chunk of delta joint angles. This design enhances temporal action consistency, leading to higher success rates across all planning tasks.

We also generate an out-of-distribution workspace using MotionGeneralizer to further evaluate the performance of $M\pi$ NetsFusion against benchmark planners, as shown in Figure 8 and summarized in Table IV. The planning results in this workspace follow the same performance trends observed in the held-out planning tasks.

TABLE IV: Planning performance of $M\pi$ NetsFusion and baseline planners within an out-of-distribution environment (**Scene**) generated by MotionGeneralizer. “T” denotes *planning time*, “N_r” denotes percentage of planning problems reached the goal, and “S” refers to success rate. ↓ indicates lower is better, and ↑ indicates higher is better.

	AIT* [63]		MPNet [16]		SIMPNet [4]		NeuralMP [8]			M π NetsFusion		
	T [s] ↓	S [%] ↑	T [s] ↓	S [%] ↑	T [s] ↓	S [%] ↑	T [s] ↓	N _r [%] ↑	S [%] ↑	T [s] ↓	N _r [%] ↑	S [%] ↑
Scene	1.02±0.0	31%	5.81±4.30	36%	7.21±10.58	38%	0.87±0.0	1.0%	1.0%	0.28±0.02	100%	28%

TABLE V: Planning comparison between $M\pi$ NetsFusion and different frameworks that differently combine planning sensing modalities. “N_r” denotes percentage of planning problems reached the goal, and “S” denotes *success rate*. ↑ indicates higher is better. “ π -All” denotes $M\pi$ NetsFusion - Planning Embeddings Considered Separately, and “ π -Config” refers to $M\pi$ NetsFusion - Configuration Space Embeddings Combined.

	TableTop		Box		Bins		Shelf					
	N _r [%] ↑	S [%] ↑	N _r [%] ↑	S [%] ↑	N _r [%] ↑	S [%] ↑	Task I		Task II		Task III	
	N _r [%] ↑	S [%] ↑	N _r [%] ↑	S [%] ↑	N _r [%] ↑	S [%] ↑	N _r [%] ↑	S [%] ↑	N _r [%] ↑	S [%] ↑	N _r [%] ↑	S [%] ↑
ACT [20], [38]	87%	37%	86%	51%	88.5%	65.25%	69.66%	30.6%	74%	27%	85.3%	28.3%
π -All	96%	49%	97.6%	61%	100%	86.75%	100%	34%	95%	31%	93%	36.6%
π -Config	100%	57%	99.3%	60.3%	100%	85%	100%	40.3%	98.3%	34%	93.3%	40.6%
ViTacFormer [64]	100%	57%	100%	62%	100%	85.75%	100%	35.6%	98.3%	34.6%	99.33%	33.33%
MπNetsFusion	100%	58%	100%	61.3%	100%	84.5%	100%	38%	100%	34.3%	97.3%	38.3%

H. Ablation Studies

In this section, we compare the performance of $M\pi$ NetsFusion against ablations of its components and architecture to evaluate the contribution and impact of each module on overall performance.

TABLE VI: Network parameter size and cold-start time comparison between $M\pi$ NetsFusion and ablative structures.

	Cold Start [ms] ↓	Network Size
ACT [20], [38]	3.8	4.52M
π -All	7	7.32M
π -Config	4.6	4.55M
ViTacFormer [64]	5.01	4.6M
MπNetsFusion	4.1	4.15M

Combining Planning Modalities: In this part, we compare the performance of $M\pi$ NetsFusion against different frameworks with specific architectures for combining motion planning sensing modalities (i.e., robotic manipulator and workspace sensing information). These frameworks are as follows:

Action Chunking Transformers (ACT): This framework is inspired by [20] and concurrent work [38], which contains an encoder-decoder transformer architecture to predict feature joint angles given workspace and configuration space embeddings. This framework combines various planning sensing modalities through a vanilla attention mechanism for motion planning. We adopt this framework for the UR5e robotic manipulator to compare the performance with $M\pi$ NetsFusion. Figure 9 demonstrates the structure of this framework.

$M\pi$ NetsFusion - Planning Embeddings Considered Separately: In this case, we consider the current and goal configuration embeddings, the robot point cloud embedding, and workspace point cloud embedding as separate inputs to the

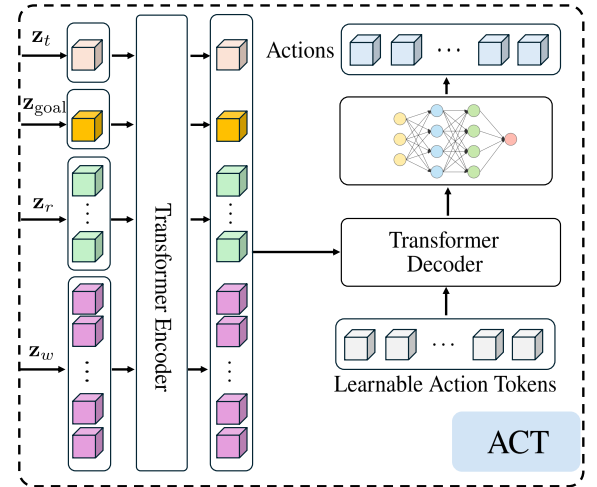


Fig. 9: ACT Network Architecture [20], [38]. The framework leverages current-time-step workspace information (including the workspace and robot point clouds) together with configuration space features (current-time-step and goal configurations) through a standard pair-wise attention mechanism to generate an action sequence that guides the robotic manipulator toward the motion planning goal. z_t , z_{goal} , z_r , and z_w are the current time-step configuration, planning goal configuration, robot point cloud, and scene point cloud embeddings, respectively.

transformer encoder such that these embeddings can only communicate through bottleneck tokens within the transformer encoder. As a result, the fusion transformer attends to four motion planning modalities instead of the original two.

$M\pi$ NetsFusion - Configuration Space Embeddings Combined: Instead of considering separate tokens for representing current and goal configuration embeddings, we first concatenate their embeddings and consider it as a single input to the transformer encoder. In this case, the fusion transformer attends to three motion planning modalities instead of the original two, which are configuration space embeddings, robot point cloud embedding, and workspace point cloud embedding, to communicate

TABLE VII: Planning comparison between M π NetsFusion and ablation frameworks with different action chunk sizes in terms of planning time and success rate. “ π ” stands for M π NetsFusion.

	TableTop		Box		Bins		Shelf					
	T [s] ↓	S [%] ↑	T [s] ↓	S [%] ↑	T [s] ↓	S [%] ↑	Task I		Task II		Task III	
#1	1.38±0.05	55%	1.36±0.06	57%	1.34±0.06	82%	1.38±0.05	35%	1.39±0.02	32%	1.41±0.05	36%
#5	0.44±0.02	57%	0.49±0.05	60%	0.47±0.07	81%	0.47±0.03	30%	0.46±0.06	34%	0.47±0.05	37%
#20	0.29±0.07	52%	0.34±0.05	60%	0.3±0.05	83%	0.3±0.04	35%	0.28±0.01	32%	0.28±0.01	40%
π (#10)	0.22±0.01	58%	0.23±0.05	61.3%	0.24±0.04	84.5%	0.24±0.03	35.7%	0.22±0.01	34.6%	0.22±0.01	33.4%

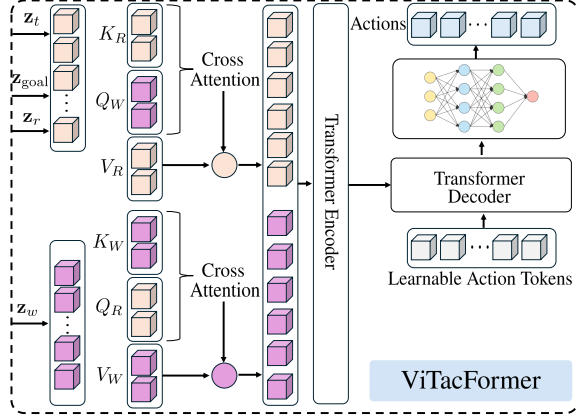


Fig. 10: ViTacFormer Network Architecture [64]. The framework utilizes a cross-attention mechanism to learn the interaction between planning sensing modalities. z_t , z_{goal} , z_r , and z_w are the current time-step configuration, planning goal configuration, robot point cloud, and scene point cloud embeddings, respectively. K_R , Q_R , and V_R are the robot embedding’s key, query, and value matrices, respectively. K_W , Q_W , and V_W are workspace embedding’s key, query, and value matrices, respectively.

TABLE VIII: Average success rate and time comparison of M π NetsFusion with planners with different action chunk sizes across all held-out planning tasks. “ π ” denotes M π NetsFusion.

		#1	#5	#20	π (#10)
	T	6.27	2.0	1.31	1.0
T_{Fusion}	TableTop	6.27	2.0	1.31	1.0
	Box	5.91	2.13	1.47	1.0
	Bins	5.58	1.95	1.25	1.0
	Shelf I	5.57	1.95	1.25	1.0
	Shelf II	6.31	2.09	1.27	1.0
	Shelf III	6.40	2.13	1.27	1.0
	Average	6	2.04	1.3	1.0



Fig. 11: Experimental Setup for real-world deployment of M π NetsFusion on UR5e robotic manipulator. The calibrated RGB-D camera is an Intel RealSense D435i used to capture workspace observations.

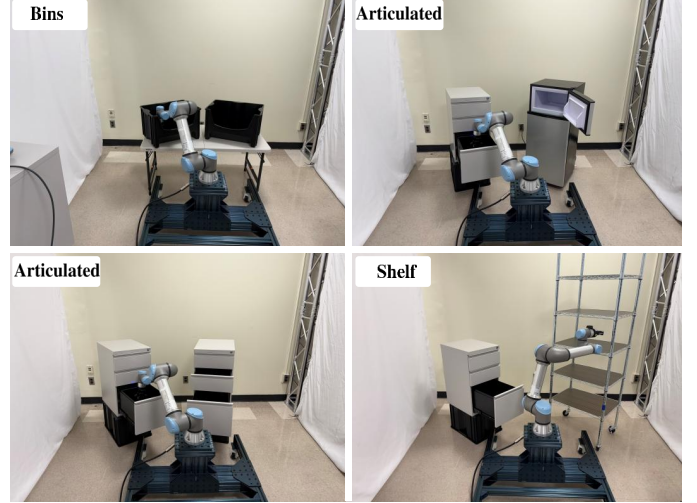


Fig. 12: Evaluation Tasks for M π NetsFusion real-world deployment.

through bottleneck tokens.

ViTacFormer [64]: Originally proposed for learning cross-modal representations in visuo-tactile manipulation, this framework employs a cross-attention mechanism to model interactions between different sensing modalities. We adopt this approach to learn and encode the relationships among various planning sensing modalities. Similar to SIMPNet [4] and M π NetsFusion, we concatenate the current time step and goal configuration embeddings with robot point cloud embeddings as a single planning modality, and utilize the cross-attention mechanism to learn the interaction between these sensing modalities as shown in Figure 10.

For comparison, we report the success rate, reaching goal, and cold start time (CS) of each structure. Cold start time is defined as the average time to respond to a new problem, which is a metric to measure reactivity to a new planning problem.

M π NetsFusion outperforms ACT in both goal-reaching and success rate across all evaluation tasks, as shown in Table V. ACT models the interaction between planning modalities using a standard attention mechanism, which often causes the workspace point-cloud embedding to dominate in evaluation static environments. In contrast, M π NetsFusion utilizes bottleneck tokens to learn interactions between robot and workspace planning embeddings, which leads to more efficient motion planning. M π NetsFusion also performs comparably to ACT

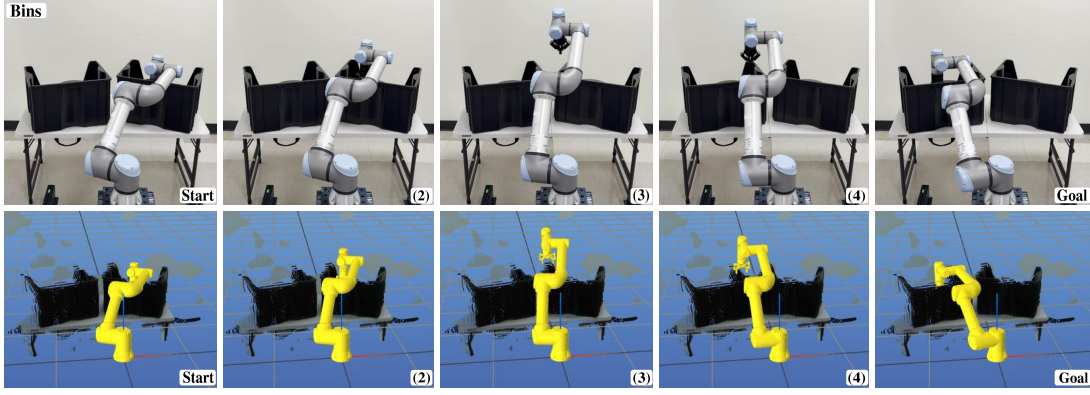


Fig. 13: Bins Task Evaluation of $M\pi$ NetsFusion in the real-world. The path profile from the start configuration to the goal configuration is demonstrated through frames 2-4 in the real-world (top), and simulated scene point cloud (bottom).

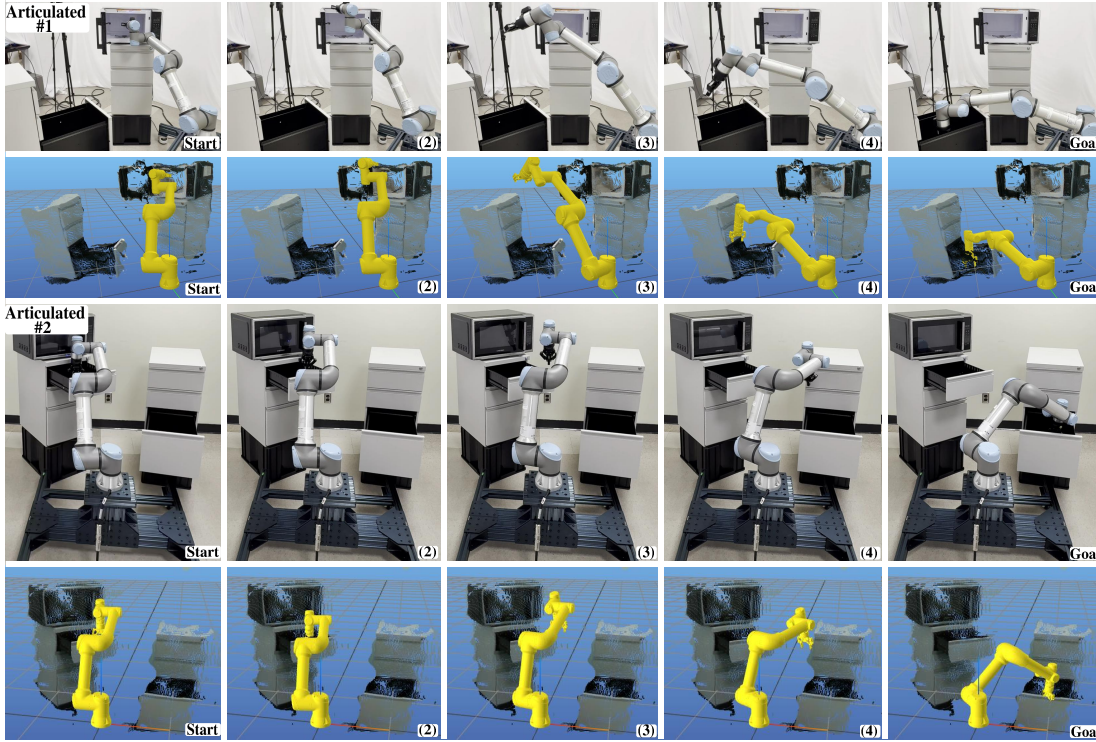


Fig. 14: Articulated Task Evaluation of $M\pi$ NetsFusion in the real-world. The path profile from the start configuration to the goal configuration is demonstrated through frames 2-4 in the real-world (top), and simulated scene point cloud (bottom).

in terms of cold-start time, as shown in Table VI, which is due to the fact that both models share the same network size.

π -Config and π -All are variants of $M\pi$ NetsFusion that further separate the planning modalities, allowing them to communicate through bottleneck tokens rather than simple concatenation. As shown in Table V, their performance is comparable to $M\pi$ NetsFusion. However, both variants exhibit higher cold-start times, which can be attributed to their larger model sizes as demonstrated in Table VI.

The ViTacFormer framework also performs comparably to $M\pi$ NetsFusion in terms of goal reaching, success rate, and cold-start time, as shown in Tables V and VI. Its performance further supports the claim that explicitly processing robot-related and workspace-embedding signals enhances the

efficiency of neural motion planners.

Action Chunk: Since $M\pi$ NetsFusion is an open-loop planner that unrolls the policy for a fixed number of steps, we vary the action-chunk size to assess its effect on planning accuracy. We evaluate chunk sizes of 1, 5, 10, and 20 to examine how different values influence performance. Because the planner operates in an open-loop, end-to-end manner, the rollout length is kept fixed across all experiments for consistency, such that models with action chunks of 1, 5, 10, and 20 are rolled out for 100, 20, 10, and 5 steps. Table VII demonstrates the performance of the planner with different action chunk sizes across all evaluation planning tasks, while Table VIII provides average time comparison between these planners.

As shown in Table VII, $M\pi$ NetsFusion with an action-chunk

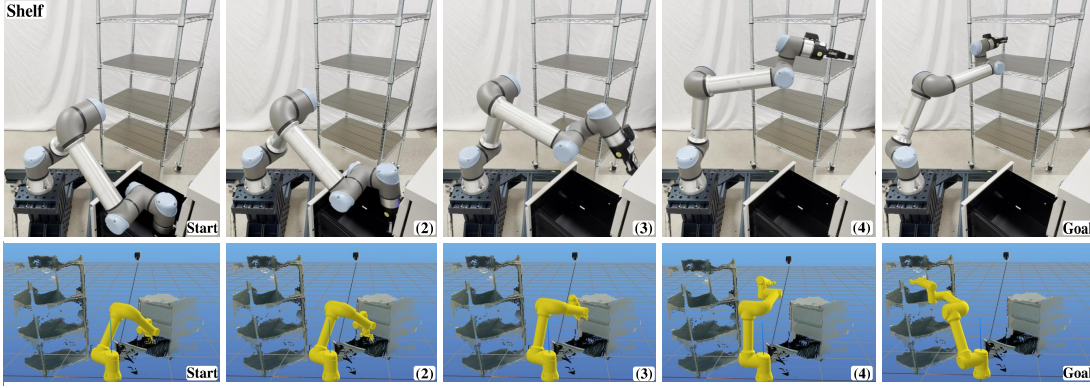


Fig. 15: Shelf Task Evaluation of $M\pi$ NetsFusion in the real-world. The path profile from the start configuration to the goal configuration is demonstrated through frames 2-4 in the real-world (top), and simulated scene point cloud (bottom).

size of 10 achieves a success rate comparable to the policy version using a chunk size of 1. This is expected because the environments are static, and both planners produce trajectories of equal length under the max rollout assumption. However, the main framework is approximately six times faster than the model with an action chunk of size 1, as demonstrated in Table VIII. This improvement arises because the policy with a chunk size of 1 must sample the robot’s body point cloud in more steps, which results in higher planning times.

A similar pattern is observed when comparing the policy with an action-chunk size of 5 to the main model. As shown in Table VII, both achieve comparable success rates. However, the main policy is at least twice as fast as the policy with an action chunk size of 5, as demonstrated in Table VIII. This planning time difference arises since the policy with an action chunk of size 10 necessitates more point-cloud sampling on the body of the robotic manipulator during inference.

The main policy (π #10) also performs comparably to the model with an action chunk size of 20 (see Table VII), which is expected given the open-loop nature of the planners. However, the main policy is slightly faster (1.3 \times) than the policy with an action chunk size of 20, despite requiring fewer point cloud sampling steps on the body of the robotic manipulator. This performance gap can be traced back to the data-processing stage: when training with an action chunk size of 20, many dataset trajectory segments require post-pended zero-masked values for the delta-joint actions. These padded sequences increase the effective inference time of the motion planner.

VI. REAL-WORLD DEPLOYMENT

In this section, we evaluate our motion policy on a UR5e robotic manipulator in real-world environments. One or two calibrated Intel RealSense D435i RGB-D cameras are used to capture point cloud data of the environment, as illustrated in Figure 11.

The real-world tasks follow the structure of some held-out evaluation tasks described in Section V as demonstrated in Figure 12. We categorize these tasks into three groups: the **Bin Task**, **Articulated Task**, and **Shelf Task**. Table IX summarizes the planning results for these real-world tasks, and Figures

13, 14, and 15 demonstrate planning examples for each task category.

TABLE IX: $M\pi$ NetsFusion performance in real-world evaluation tasks, reported using **ReachedGoal** and **Successful** metrics.

	Bins	Articulated	Shelf	Total #	Total [%]
ReachedGoal \uparrow	10/10	17/17	10/10	37/37	100%
Successful \uparrow	8/10	11/17	3/10	22/37	59.4%

For the bins tasks, the planner reaches the planning goal in all the planning problems (10/10), among which 8 are successful and collision-free. These results are consistent with the simulation performance on the bins tasks. For the articulated tasks, the planner also reaches the planning goal in all the planning problems (17/17), among which 11 are successful and collision-free. For the shelf task, the planner reaches the planning goal in all the planning problems (10/10); however, only 3 out of 10 are successful and collision-free. These results are also consistent with the simulation performance on the shelf tasks.

VII. CONCLUSIONS

In this paper, we present **PerFACT**, which contains two modules to learn the motion policy for robotic manipulators. The first module, **MotionGeneralizer**, is an LLM-based workspace generation framework that is used for collecting large-scale motion planning datasets. The second module, **$M\pi$ NetsFusion**, is a novel neural motion planning framework for end-to-end motion planning for robotic manipulators. MotionGeneralizer has specific features that make it capable of generating motion-planning datasets for any robotic manipulator with arbitrary degrees of freedom (DOF). These features are as follows:

Diverse Workspace generation: MotionGeneralizer leverages procedural everyday geometric primitives generation with the semantic reasoning capabilities of LLMs to create feasible and cluttered workspaces around robotic manipulators for motion planning. This framework utilizes a chain-of-thought (CoT) prompting technique to create workspaces with high diversity.

Robot-agnostic, scene-specific motion planning problems: MotionGeneralizer samples collision-free, robot-agnostic

tight-space poses within each workspace by considering the positions and orientations of all primitives. It then uses robot-specific inverse kinematics to compute feasible start and goal configurations for the selected robotic manipulator. The resulting planning problems can be solved by any off-the-shelf classical motion planner (e.g., OMPL [19] or cuRobo [10]) for large-scale planning dataset collection.

Sensing modality: MotionGeneralizer samples points directly on the meshes of both the workspace primitives and the robotic manipulator at arbitrary configurations, to provide planners privileged access to accurate geometric and shape information. Compared to using RGB-D cameras in simulation, this approach is faster and provides a complete representation of the planning workspace.

We then utilized the MotionGeneralizer framework to collect a large-scale dataset for training $M\pi$ NetsFusion, a novel end-to-end, open-loop motion planner for the UR5e robotic manipulators. $M\pi$ NetsFusion employs a bottleneck-based fusion transformer architecture that intelligently attends to various planning modalities. The model adopts an action-chunking transformer encoder-decoder architecture to predict future delta joint angles from the current time-step workspace and robot embedding information. The encoder is designed so that the robot and workspace embeddings communicate only through bottleneck tokens, which aggregate and balance the planning information while preventing the workspace embedding from dominating the planning signal.

We compare the performance of the proposed planner with state-of-the-art sampling-based and neural motion planners. The evaluation results demonstrate that $M\pi$ NetsFusion achieves superior average planning time and comparable success rate relative to benchmark methods across all held-out planning tasks. Our ablation studies also demonstrate that treating the robotic manipulator and scene embeddings separately-instead of simple concatenation-yields substantial performance improvements. Additional separation of the robotic manipulator’s configuration space and workspace information yields only marginal performance gains while increasing model size and cold-start time. Additionally, we showcase that action chunking significantly reduces the overall planning time due to the end-to-end nature of the proposed framework. Finally, our experimental results highlight the planner’s performance across a range of real-world planning tasks.

However, our proposed MotionGeneralizer and $M\pi$ NetsFusion have several limitations that will be potential research directions for our future work. MotionGeneralizer relies on prompting an LLM to describe each workspace for similarity estimation. However, similarity between language descriptions of generated workspaces does not necessarily reflect the true geometric similarity between workspaces. Vision-based similarity metrics have the potential to provide more accurate similarity detection measures and could further improve MotionGeneralizer to generate more diverse workspaces. Also, this framework only considers articulated primitives for workspace creation. Incorporating existing 3D datasets like Objaverse [14] to sample simple everyday

meshes to place between, within, or on top of the generated articulated primitives would produce more realistic and cluttered environments.

Also, $M\pi$ NetsFusion is currently limited to static environments due to its end-to-end, open-loop design. To extend its applicability to dynamic environments, a high-frequency reactive motion planner like Riemannian Motion Policies (RMPs) [65] or Geometric Fabrics [66] would need to operate on top of $M\pi$ NetsFusion to handle environmental changes in real time. Additionally, although MotionGeneralizer enables the collection of motion planning data for robotic manipulators with arbitrary degrees of freedom, $M\pi$ NetsFusion is trained and evaluated only for the UR5e manipulator. Thus, the proposed motion planner is embodiment-specific and cannot be directly applied to other robotic manipulators with different degrees of freedom.

VIII. ACKNOWLEDGMENTS

This work was supported by the USA National Science Foundation under Grant No. 2026533/2422826. Portions of this research were conducted with the advanced computing resources provided by Texas A&M High Performance Research Computing.

REFERENCES

- [1] S. M. LaValle, *Planning algorithms*. Cambridge university press, 2006.
- [2] A. Orthey, C. Chamzas, and L. E. Kavraki, “Sampling-based motion planning: A comparative review,” *Annual Review of Control, Robotics, and Autonomous Systems*, vol. 7, 2023.
- [3] M. Zucker, N. Ratliff, A. D. Dragan, M. Pivtoraiko, M. Klingensmith, C. M. Dellin, J. A. Bagnell, and S. S. Srinivasa, “Chomp: Covariant hamiltonian optimization for motion planning,” *The International journal of robotics research*, vol. 32, no. 9-10, pp. 1164–1193, 2013.
- [4] D. Soleymanzadeh, X. Liang, and M. Zheng, “Simpnet: Spatial-informed motion planning network,” *IEEE Robotics and Automation Letters*, 2025.
- [5] Farber, “Topological complexity of motion planning,” *Discrete & Computational Geometry*, vol. 29, pp. 211–221, 2003.
- [6] C. Chamzas, Z. Kingston, C. Quintero-Peña, A. Shrivastava, and L. E. Kavraki, “Learning sampling distributions using local 3d workspace decompositions for motion planning in high dimensions,” in *2021 IEEE International Conference on Robotics and Automation (ICRA)*. IEEE, 2021, pp. 1283–1289.
- [7] C. Chamzas, C. Quintero-Peña, Z. Kingston, A. Orthey, D. Rakita, M. Gleicher, M. Toussaint, and L. E. Kavraki, “Motionbenchmarker: A tool to generate and benchmark motion planning datasets,” *IEEE Robotics and Automation Letters*, vol. 7, no. 2, pp. 882–889, 2021.
- [8] M. Dalal, J. Yang, R. Mendonca, Y. Khaky, R. Salakhutdinov, and D. Pathak, “Neural mp: A generalist neural motion planner,” *arXiv preprint arXiv:2409.05864*, 2024.
- [9] J. Achiam, S. Adler, S. Agarwal, L. Ahmad, I. Akkaya, F. L. Aleman, D. Almeida, J. Altenschmidt, S. Altman, S. Anadkat *et al.*, “Gpt-4 technical report (2023),” *arXiv preprint arXiv:2303.08774*, 2023.
- [10] B. Sundaralingam, S. K. S. Hari, A. Fishman, C. Garrett, K. Van Wyk, V. Blukis, A. Millane, H. Oleynikova, A. Handa, F. Ramos *et al.*, “Curobo: Parallelized collision-free robot motion generation,” in *2023 IEEE International Conference on Robotics and Automation (ICRA)*. IEEE, 2023, pp. 8112–8119.
- [11] Y. Wang, Z. Xian, F. Chen, T.-H. Wang, Y. Wang, K. Fragkiadaki, Z. Erickson, D. Held, and C. Gan, “Robogen: Towards unleashing infinite data for automated robot learning via generative simulation,” in *International Conference on Machine Learning*. PMLR, 2024, pp. 51 936–51 983.
- [12] W. X. Zhao, K. Zhou, J. Li, T. Tang, X. Wang, Y. Hou, Y. Min, B. Zhang, J. Zhang, Z. Dong *et al.*, “A survey of large language models,” *arXiv preprint arXiv:2303.18223*, vol. 1, no. 2, 2023.

- [13] L. Wang, C. Ma, X. Feng, Z. Zhang, H. Yang, J. Zhang, Z. Chen, J. Tang, X. Chen, Y. Lin *et al.*, "A survey on large language model based autonomous agents," *Frontiers of Computer Science*, vol. 18, no. 6, p. 186345, 2024.
- [14] M. Deitke, D. Schwenk, J. Salvador, L. Weihs, O. Michel, E. VanderBilt, L. Schmidt, K. Ehsani, A. Kembhavi, and A. Farhadi, "Objaverse: A universe of annotated 3d objects," in *Proceedings of the IEEE/CVF conference on computer vision and pattern recognition*, 2023, pp. 13 142–13 153.
- [15] H. Wang, X. Du, J. Li, R. A. Yeh, and G. Shakhnarovich, "Score jacobian chaining: Lifting pretrained 2d diffusion models for 3d generation," in *Proceedings of the IEEE/CVF conference on computer vision and pattern recognition*, 2023, pp. 12 619–12 629.
- [16] A. H. Qureshi, A. Simeonov, M. J. Bency, and M. C. Yip, "Motion planning networks," in *2019 International Conference on Robotics and Automation (ICRA)*. IEEE, 2019, pp. 2118–2124.
- [17] A. Fishman, A. Murali, C. Eppner, B. Peele, B. Boots, and D. Fox, "Motion policy networks," in *conference on Robot Learning*. PMLR, 2023, pp. 967–977.
- [18] C. Eppner, A. Murali, C. Garrett, R. O'Flaherty, T. Hermans, W. Yang, and D. Fox, "scene_synthesizer: A python library for procedural scene generation in robot manipulation," *Journal of Open Source Software*, vol. 10, no. 105, p. 7561, 2025.
- [19] I. A. Sucan, M. Moll, and L. E. Kavraki, "The open motion planning library," *IEEE Robotics & Automation Magazine*, vol. 19, no. 4, pp. 72–82, 2012.
- [20] T. Z. Zhao, V. Kumar, S. Levine, and C. Finn, "Learning fine-grained bimanual manipulation with low-cost hardware," *arXiv preprint arXiv:2304.13705*, 2023.
- [21] A. Nagrani, S. Yang, A. Arnab, A. Jansen, C. Schmid, and C. Sun, "Attention bottlenecks for multimodal fusion," *Advances in neural information processing systems*, vol. 34, pp. 14 200–14 213, 2021.
- [22] C. Higuera, A. Sharma, T. Fan, C. K. Bodduluri, B. Boots, M. Kaess, M. Lambeta, T. Wu, Z. Liu, F. R. Hogan *et al.*, "Tactile beyond pixels: Multisensory touch representations for robot manipulation," *arXiv preprint arXiv:2506.14754*, 2025.
- [23] M. J. Bency, A. H. Qureshi, and M. C. Yip, "Neural path planning: Fixed time, near-optimal path generation via oracle imitation," in *2019 IEEE/RSJ International Conference on Intelligent Robots and Systems (IROS)*. IEEE, 2019, pp. 3965–3972.
- [24] Z. Liu, Y. Feng, M. J. Black, D. Nowrouzezahrai, L. Paull, and W. Liu, "Meshdiffusion: Score-based generative 3d mesh modeling," *arXiv preprint arXiv:2303.08133*, 2023.
- [25] X. Long, Y.-C. Guo, C. Lin, Y. Liu, Z. Dou, L. Liu, Y. Ma, S.-H. Zhang, M. Habermann, C. Theobalt *et al.*, "Wonder3d: Single image to 3d using cross-domain diffusion," in *Proceedings of the IEEE/CVF conference on computer vision and pattern recognition*, 2024, pp. 9970–9980.
- [26] Y. Hu, L. Wang, X. Liu, L.-H. Chen, Y. Guo, Y. Shi, C. Liu, A. Rao, Z. Wang, and H. Xiong, "Simulating the real world: A unified survey of multimodal generative models," *arXiv preprint arXiv:2503.04641*, 2025.
- [27] F. Xiang, Y. Qin, K. Mo, Y. Xia, H. Zhu, F. Liu, M. Liu, H. Jiang, Y. Yuan, H. Wang *et al.*, "Sapien: A simulated part-based interactive environment," in *Proceedings of the IEEE/CVF conference on computer vision and pattern recognition*, 2020, pp. 11 097–11 107.
- [28] S. Nasiriany, A. Maddukuri, L. Zhang, A. Parikh, A. Lo, A. Joshi, A. Mandlekar, and Y. Zhu, "Robocasa: Large-scale simulation of everyday tasks for generalist robots," *arXiv preprint arXiv:2406.02523*, 2024.
- [29] A. Kirillov, E. Mintun, N. Ravi, H. Mao, C. Rolland, L. Gustafson, T. Xiao, S. Whitehead, A. C. Berg, W.-Y. Lo *et al.*, "Segment anything," in *Proceedings of the IEEE/CVF international conference on computer vision*, 2023, pp. 4015–4026.
- [30] L. H. Li, P. Zhang, H. Zhang, J. Yang, C. Li, Y. Zhong, L. Wang, L. Yuan, L. Zhang, J.-N. Hwang *et al.*, "Grounded language-image pre-training," in *Proceedings of the IEEE/CVF conference on computer vision and pattern recognition*, 2022, pp. 10 965–10 975.
- [31] Y. Chen, J. Arkin, C. Dawson, Y. Zhang, N. Roy, and C. Fan, "Autotamp: Autoregressive task and motion planning with llms as translators and checkers," in *2024 IEEE International conference on robotics and automation (ICRA)*. IEEE, 2024, pp. 6695–6702.
- [32] J. Liang, W. Huang, F. Xia, P. Xu, K. Hausman, B. Ichter, P. Florence, and A. Zeng, "Code as policies: Language model programs for embodied control," in *2023 IEEE International Conference on Robotics and Automation (ICRA)*. IEEE, 2023, pp. 9493–9500.
- [33] W. Huang, C. Wang, R. Zhang, Y. Li, J. Wu, and L. Fei-Fei, "Voxposer: Composable 3d value maps for robotic manipulation with language models," *arXiv preprint arXiv:2307.05973*, 2023.
- [34] T. Kwon, N. Di Palo, and E. Johns, "Language models as zero-shot trajectory generators," *IEEE Robotics and Automation Letters*, 2024.
- [35] B. Zitkovich, T. Yu, S. Xu, P. Xu, T. Xiao, F. Xia, J. Wu, P. Wohlhart, S. Welker, A. Wahid *et al.*, "Rt-2: Vision-language-action models transfer web knowledge to robotic control," in *Conference on Robot Learning*. PMLR, 2023, pp. 2165–2183.
- [36] Q. Vuong, S. Levine, H. R. Walke, K. Pertsch, A. Singh, R. Doshi, C. Xu, J. Luo, L. Tan, D. Shah *et al.*, "Open x-embodiment: Robotic learning datasets and rt-x models," in *Towards Generalist Robots: Learning Paradigms for Scalable Skill Acquisition@ CoRL2023*, 2023.
- [37] K. Black, N. Brown, D. Driess, A. Esmail, M. Equi, C. Finn, N. Fusai, L. Groom, K. Hausman, B. Ichter *et al.*, "π0: A vision-language-action flow model for general robot control, 2024," URL <https://arxiv.org/abs/2410.24164>.
- [38] J. Yang, J. J. Liu, Y. Li, Y. Khaky, K. Shaw, and D. Pathak, "Deep reactive policy: Learning reactive manipulator motion planning for dynamic environments," *arXiv preprint arXiv:2509.06953*, 2025.
- [39] T. Lai and F. Ramos, "Plannerflows: Learning motion samplers with normalising flows," in *2021 IEEE/RSJ International Conference on Intelligent Robots and Systems (IROS)*. IEEE, 2021, pp. 2542–2548.
- [40] J. J. Johnson, A. H. Qureshi, and M. C. Yip, "Learning sampling dictionaries for efficient and generalizable robot motion planning with transformers," *IEEE Robotics and Automation Letters*, vol. 8, no. 12, pp. 7946–7953, 2023.
- [41] —, "Zero-shot constrained motion planning transformers using learned sampling dictionaries," in *2024 IEEE International Conference on Robotics and Automation (ICRA)*. IEEE, 2024, pp. 14 363–14 369.
- [42] M. Song, Y. Kim, M. J. Kim, and D. Park, "Graph-based 3d collision-distance estimation network with probabilistic graph rewiring," in *2024 IEEE International Conference on Robotics and Automation (ICRA)*. IEEE, 2024, pp. 10 939–10 945.
- [43] Y. Kim, J. Kim, and D. Park, "Graphdistnet: A graph-based collision-distance estimator for gradient-based trajectory optimization," *IEEE Robotics and Automation Letters*, vol. 7, no. 4, pp. 11 118–11 125, 2022.
- [44] A. Krawczyk, J. Marciniak, and D. Belter, "Comparison of machine learning techniques for self-collisions checking of manipulating robots," in *2023 27th International Conference on Methods and Models in Automation and Robotics (MMAR)*. IEEE, 2023, pp. 472–477.
- [45] A. Murali, A. Mousavian, C. Eppner, A. Fishman, and D. Fox, "Cabinet: Scaling neural collision detection for object rearrangement with procedural scene generation," *arXiv preprint arXiv:2304.09302*, 2023.
- [46] S. Park, S. Jeon, and J. Park, "A constrained motion planning method exploiting learned latent space for high-dimensional state and constraint spaces," *IEEE/ASME Transactions on Mechatronics*, vol. 29, no. 4, pp. 3001–3009, 2024.
- [47] T. S. Lembono, E. Pignat, J. Jankowski, and S. Calinon, "Learning constrained distributions of robot configurations with generative adversarial network," *IEEE Robotics and Automation Letters*, vol. 6, no. 2, pp. 4233–4240, 2021.
- [48] J. Ichnowski, Y. Avigal, V. Satish, and K. Goldberg, "Deep learning can accelerate grasp-optimized motion planning," *Science Robotics*, vol. 5, no. 48, p. eabd7710, 2020.
- [49] J. Carvalho, A. T. Le, M. Baierl, D. Koert, and J. Peters, "Motion planning diffusion: Learning and planning of robot motions with diffusion models," in *2023 IEEE/RSJ International Conference on Intelligent Robots and Systems (IROS)*. IEEE, 2023, pp. 1916–1923.
- [50] S. Yan, Z. Zhang, M. Han, Z. Wang, Q. Xie, Z. Li, Z. Li, H. Liu, X. Wang, and S.-C. Zhu, "M 2 diffuser: Diffusion-based trajectory optimization for mobile manipulation in 3d scenes," *IEEE Transactions on Pattern Analysis and Machine Intelligence*, 2025.
- [51] K. Saha, V. Mandadi, J. Reddy, A. Srikanth, A. Agarwal, B. Sen, A. Singh, and M. Krishna, "Edmp: Ensemble-of-costs-guided diffusion for motion planning," in *2024 IEEE International Conference on Robotics and Automation (ICRA)*. IEEE, 2024, pp. 10 351–10 358.
- [52] A. H. Qureshi, Y. Miao, A. Simeonov, and M. C. Yip, "Motion planning networks: Bridging the gap between learning-based and classical motion planners," *IEEE Transactions on Robotics*, vol. 37, no. 1, pp. 48–66, 2020.
- [53] A. H. Qureshi, J. Dong, A. Choe, and M. C. Yip, "Neural manipulation planning on constraint manifolds," *IEEE Robotics and Automation Letters*, vol. 5, no. 4, pp. 6089–6096, 2020.
- [54] A. H. Qureshi, J. Dong, A. Baig, and M. C. Yip, "Constrained motion planning networks x," *IEEE Transactions on Robotics*, vol. 38, no. 2, pp. 868–886, 2021.
- [55] C. W. Ramsey, Z. Kingston, W. Thomason, and L. E. Kavraki, "Collision-affording point trees: Simd-amenable nearest neighbors for fast collision checking," *arXiv preprint arXiv:2406.02807*, 2024.

- [56] T. G. W. Lum, M. Matak, V. Makoviychuk, A. Handa, A. Allshire, T. Hermans, N. D. Ratliff, and K. Van Wyk, "Dextrah-g: Pixels-to-action dexterous arm-hand grasping with geometric fabrics," in *8th Annual Conference on Robot Learning*.
- [57] C. Chi, Z. Xu, S. Feng, E. Cousineau, Y. Du, B. Burchfiel, R. Tedrake, and S. Song, "Diffusion policy: Visuomotor policy learning via action diffusion," *The International Journal of Robotics Research*, vol. 44, no. 10-11, pp. 1684–1704, 2025.
- [58] L. Lai, A. Z. Huang, and S. J. Gershman, "Action chunking as policy compression," *PsyArXiv*, 2022.
- [59] C. R. Qi, L. Yi, H. Su, and L. J. Guibas, "Pointnet++: Deep hierarchical feature learning on point sets in a metric space," *Advances in neural information processing systems*, vol. 30, 2017.
- [60] A. Dosovitskiy, "An image is worth 16x16 words: Transformers for image recognition at scale," *arXiv preprint arXiv:2010.11929*, 2020.
- [61] A. Paszke, S. Gross, S. Chintala, G. Chanan, E. Yang, Z. DeVito, Z. Lin, A. Desmaison, L. Antiga, and A. Lerer, "Automatic differentiation in pytorch," 2017.
- [62] M. Dalal, M. Liu, W. Talbott, C. Chen, D. Pathak, J. Zhang, and R. Salakhutdinov, "Local policies enable zero-shot long-horizon manipulation," *arXiv preprint arXiv:2410.22332*, 2024.
- [63] M. P. Strub and J. D. Gammell, "Adaptively informed trees (ait*): Fast asymptotically optimal path planning through adaptive heuristics," in *2020 IEEE International Conference on Robotics and Automation (ICRA)*. IEEE, 2020, pp. 3191–3198.
- [64] L. Heng, H. Geng, K. Zhang, P. Abbeel, and J. Malik, "Vitacformer: Learning cross-modal representation for visuo-tactile dexterous manipulation," *arXiv preprint arXiv:2506.15953*, 2025.
- [65] N. D. Ratliff, J. Issac, D. Kappler, S. Birchfield, and D. Fox, "Riemannian motion policies," *arXiv preprint arXiv:1801.02854*, 2018.
- [66] K. Van Wyk, M. Xie, A. Li, M. A. Rana, B. Babich, B. Peele, Q. Wan, I. Akinola, B. Sundaralingam, D. Fox *et al.*, "Geometric fabrics: Generalizing classical mechanics to capture the physics of behavior," *IEEE Robotics and Automation Letters*, vol. 7, no. 2, pp. 3202–3209, 2022.